Ann. N.Y. Acad. Sci. ISSN 0077-89

ANNALS OF THE NEW YORK ACADEMY OF SCIENCES
Special Issue: *Antimicrobial Therapeutics Reviews*
REVIEW

AcrB: a mean, keen, drug efflux machine

Jessica Kobylka,[a] Miriam S. Kuth,[a] Reinke T. Müller,[a] Eric R. Geertsma, and Klaas M. Pos

Institute of Biochemistry, Goethe-University Frankfurt, Frankfurt am Main, Germany

Address for correspondence: Klaas M. Pos, Institute of Biochemistry, Goethe-University Frankfurt, Max-von-Laue-Str. 9, D-60438 Frankfurt am Main, Germany. pos@em.uni-frankfurt.de

Gram-negative bacteria are intrinsically resistant against cytotoxic substances by means of their outer membrane and a network of multidrug efflux systems, acting in synergy. Efflux pumps from various superfamilies with broad substrate preferences sequester and pump drugs across the inner membrane to supply the highly polyspecific and powerful tripartite resistance–nodulation–cell division (RND) efflux pumps with compounds to be extruded across the outer membrane barrier. In *Escherichia coli*, the tripartite efflux system AcrAB–TolC is the archetype RND multiple drug efflux pump complex. The homotrimeric inner membrane component acriflavine resistance B (AcrB) is the drug specificity and energy transduction center for the drug/proton antiport process. Drugs are bound and expelled via a cycle of mainly three consecutive states in every protomer, constituting a flexible alternating access channel system. This review recapitulates the molecular basis of drug and inhibitor binding, including mechanistic insights into drug efflux by AcrB. It also summarizes 17 years of mutational analysis of the gene *acrB*, reporting the effect of every substitution on the ability of *E. coli* to confer resistance toward antibiotics (http://goethe.link/AcrBsubstitutions). We emphasize the functional robustness of AcrB toward single-site substitutions and highlight regions that are more sensitive to perturbation.

Keywords: antibiotic resistance; tripartite efflux pumps; resistance–nodulation–cell division (RND); structure/function analysis; antibiotic transporters; Gram-negative

The origins of antibiotic resistance

To develop new strategies for the treatment of multidrug-resistant pathogens, it is important to understand the fundamentals of microbial resistance, including its origin. Antimicrobial resistance is not a modern phenomenon, but rather an ancient one.[1,2] Genes encoding resistance mechanisms toward β-lactams, tetracyclines, and glycopeptide antibiotics have been isolated from 30,000-year-old permafrost sediments, and a genotype-to-phenotype study identified 18 chromosomally encoded resistance markers. These included three mechanisms previously unknown to be involved in antibiotic resistance that were identified in a bacterium (*Paenibacillus* sp. LC231) originating from a cave that had been isolated from the outside world for 4 million years. However, the origin of these genes is much older. On the basis of comparison with orthologous genes, class A β-lactamases originated up to 2.4 billion years ago.[3] For comparison, life on earth, based on findings of fossilized microorganisms, is estimated to be at least 3.77 billion years old.[4] The age of modern humans (*Homo sapiens*) most likely started around a relatively modest 300,000 years ago.[5]

It does not come as a surprise that natural antimicrobial production is evolutionary related to counteracting resistance mechanisms.[6] Most antimicrobials are secondary metabolites produced by certain fungi and bacteria. These microbes are supposed to produce and release these low molecular mass compounds to inhibit essential cellular processes of other microorganisms with whom they compete for resources. In this way, they create(d) an (evolutionary) growth advantage. Inhibition can either be bactericidal (killing of bacteria) or bacteriostatic (inhibiting bacterial growth).[7]

[a]These authors contributed equally.

doi: 10.1111/nyas.14239

Ann. N.Y. Acad. Sci. 1459 (2020) 38–68 © 2019 The Authors. *Annals of the New York Academy of Sciences* published by Wiley Periodicals, Inc. on behalf of The New York Academy of Sciences.

The production of antibiotics requires complex modular biosynthetic pathways, including many enzymes and specialized carrier proteins that are encoded in large gene clusters.[8] Most known antibiotics, including β-lactams, tetracyclines, macrolides, aminoglycosides, rifamycins, and glycopeptides, have been isolated from actinomycetes, Gram-positive facultatively aerobic soil bacteria that form fungus-like branched networks.[9] Antimicrobial producers, such as actinomycetes, must be resistant to the antibiotics they produce in order not to be killed. This correlation between production and resistance can be used when searching for new antibiotics.[10]

The resistance genes of microbial producers are often encoded on the same contiguous clusters that contain the genes for antibiotic biosynthesis; and the obvious necessity of these genes makes actinomycetes a likely origin of many resistance genes in other bacteria as well.[11,12] In natural environments, it appears relatively common for bacteria to encode resistance genes (often on plasmids), even if these organisms do not produce antibiotics themselves.[13] Further, there are "consumer" bacteria that can not only resist high concentrations of antibiotics but, in addition, can metabolize these as their sole carbon source.[14] The different resistance genes of various organisms form a genetic reservoir, the so-called "resistome,"[15] which can be mobilized via horizontal gene transfer[16] into the microbial community. Such transfer can (by detours) also include into human microbial pathogens. Comparative studies, resulting in perfect nucleotide identities between the resistance cassettes of multidrug-resistant soil bacteria and those of clinical isolates, support the hypothesis of horizontal gene transfer.[17]

There are many indications suggesting that the massive use of antibiotics has led to a significant shift in balance toward the wider spread and more pronounced forms of (multiple) antibiotic resistance.[18] In 2010, for example, an estimated 63,000 tons of these chemical products were used worldwide in livestock, a market that is responsible for approximately 80% of antibiotic consumption in the United States.[19] Most mechanisms of antibiotic resistance, especially when combined and leading to multidrug-resistant phenotypes, are associated with significant fitness costs, leading to reduced bacterial growth rates.[20] Accordingly, in the absence of antibiotic exposition, multidrug-resistant pathogens are likely to be outcompeted by microbes lacking resistance markers.[21] However, since resistant bacteria are known to acquire additional fitness cost compensatory mutations, some of the resistance markers remain within the population, even in the absence of antibiotic pressure.[20]

Targets and functional principles of antimicrobial agents

Effective antimicrobial agents target essential cellular processes, including the evolutionary conserved and complex machineries of cell wall and protein biosynthesis. The mode of action of prominent antimicrobials and counteracting cellular processes are illustrated in Figure 1. The bacterial cell wall (murein) is a multilayer mesh-like peptidoglycan structure formed by long polysaccharides that are cross-linked via short peptides. The cell wall mechanically counteracts the osmotic pressure from the cell interior and influences the shape of bacteria.

Individual steps of murein synthesis are targets of different antibiotics. β-Lactams, such as oxacillin (OXA) and piperacillin (Fig. S1, online only), covalently bind to the catalytic center of the DD-transpeptidase, preventing the enzyme to catalyze the peptidoglycan cross-linking reaction.[22] Supramolecular ribosomes are the protein factories of the cell that translate mRNA-encoded genetic information into polypeptide sequences. Evolution has resulted in many active compound classes directed against this ribosome-dependent machinery; compounds that bind either to the large 50S or the small 30S subunits of bacterial 70S ribosomes, resulting in the inhibition of protein synthesis at different stages (initiation, elongation, or termination). Macrolide antibiotics—including erythromycin (ERY) and spiramycin (Fig. S1, online only), oxazolidones, like linezolid (LIN), and amphenicol antibiotics, such as chloramphenicol (CAT)—bind to the large 50S subunit, whereas aminoglycosides, such as kanamycin (KAN), and tetracyclines, such as minocycline (MIN), bind to the small 30S subunit. Fusidic acid (FUS) interacts with a protein required for a different step of protein synthesis, elongation factor G.[23]

Other bacterial protein targets of antibiotics include the replication and transcription machinery. The most prominent being the bacterial DNA gyrase, which can be inhibited by fluoroquinolones,

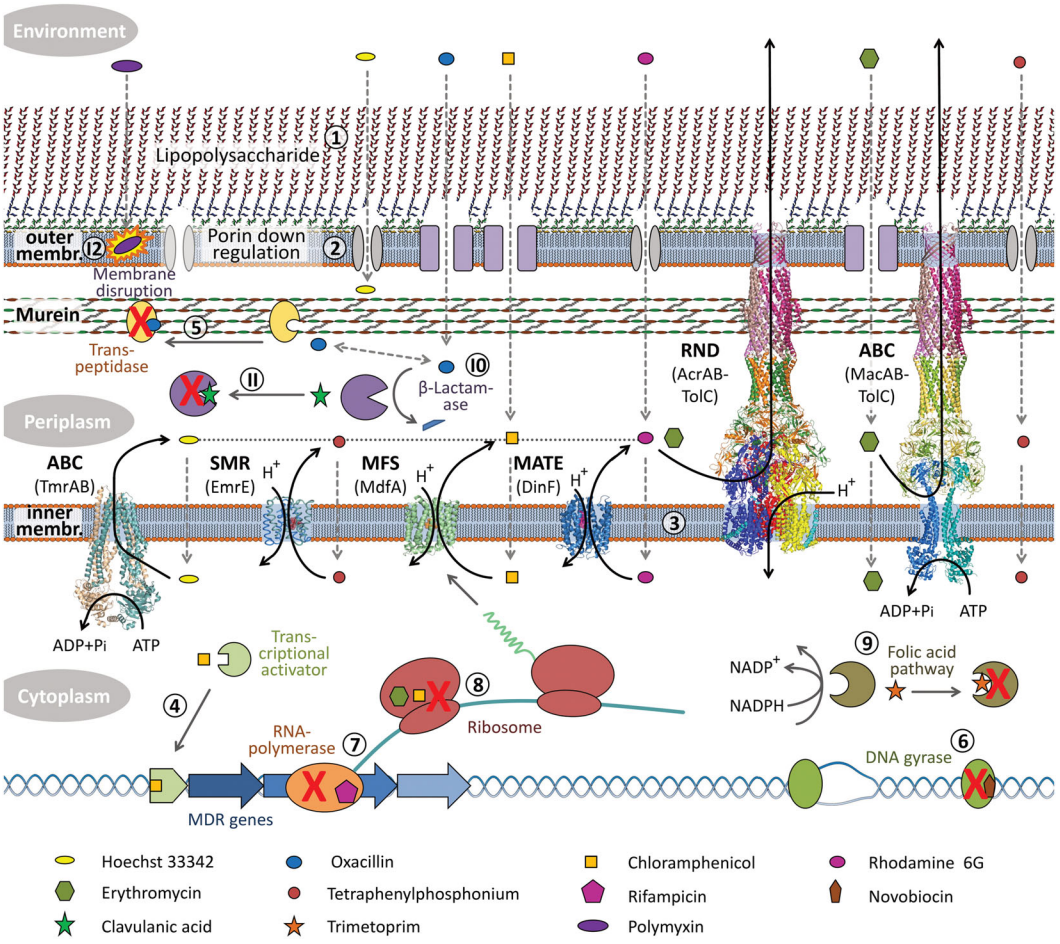

Figure 1. Multidrug-resistance efflux pumps counteract the effect of antimicrobial agents. Overview of the mode of action of several antibiotics and Gram-negative resistance mechanisms. The Gram-negative outer membrane contains a lipopolysaccharide layer, which provides a permeation barrier toward hydrophobic compounds (1). Molecules that are able to penetrate the lipopolysaccharide layer are confronted with the hydrophobic outer membrane bilayer. More hydrophilic molecules, like nutrients but also β-lactam antibiotics, enter the periplasm via porins localized in the outer membrane (2). The bacterial inner membrane (3), which separates the cytoplasm from the periplasm, poses an additional hydrophobic permeation barrier for hydrophilic compounds. Hydrophobic compounds, such as many of the known antibiotics, readily penetrate the outer leaflet of the inner membrane. The AcrAB(Z)–TolC complex, in particular the resistance nodulation and cell division (RND) component AcrB, is suggested to sequester these hydrophobic compounds from the periplasm and the outer leaflet of the inner membrane, and exports them out of the cell. This process is driven by the proton motive force present across the inner membrane. Targets for most antibiotics are located in the cytoplasm. Single-component multidrug-resistance efflux pumps of the small multidrug resistance (SMR), major facilitator (MF), multidrug and toxin extrusion (MATE), or ATP binding cassette (ABC) transporter (super)families transport antibiotics from the cytoplasm to the periplasm from where these molecules are sequestered and transported across the outer membrane by the AcrAB(Z)–TolC efflux complex. The intrinsic resistance provided by the outer membrane and the network of efflux pumps can be further increased by the downregulation of porins (2) and/or the upregulation of multidrug-resistance efflux pump genes (4). The AcrAB(Z)-TolC multidrug efflux pump recognizes many different classes of antimicrobials (Fig. S1, online only). Among those substrates are antibiotics targeting the bacterial murein (cell wall) cross-linking reaction (e.g., oxacillin (5)), DNA unwinding/replication (e.g., novobiocin (6)), DNA transcription (e.g., rifampicin (7)), the translation machinery (e.g., erythromycin, (8)), or the folic acid biosynthesis pathway (e.g., trimethoprim (9)). Besides efflux, bacterial cells can acquire further resistance mechanisms, including the enzymatic degradation of compounds (e.g., β-lactamases (10)) or by modification of target sites. Inhibitors of β-lactamases, such as clavulanic acid (11) and also polymyxins, which disrupt bacterial membranes (12), were reported to be substrates of RND homologs in Gram-negative bacteria. Under overexpressing conditions, the MacAB–TolC tripartite ABC efflux machinery was shown to confer resistance against diverse macrolide antibiotics, although its cognate function might be different.

Ann. N.Y. Acad. Sci. 1459 (2020) 38–68 © 2019 The Authors. *Annals of the New York Academy of Sciences* published by Wiley Periodicals, Inc. on behalf of The New York Academy of Sciences.

such as ciprofloxacin (CIP), and aminocoumarins, such as novobiocin (NOV),[24] and the bacterial DNA-dependent RNA-polymerase, which can be inhibited by rifampicin (RIF).[22] Metabolic pathways, such as the folic acid biosynthesis pathway that leads to the production of tetrahydrofolate, the starting compound for the synthesis of purines and pyrimidines (the base groups of RNA and DNA), can be inhibited by sulfonamides (dihydropteroate synthetase) and trimethoprim (dihydrofolate reductase).[7] Interestingly, for some antimicrobial agents, additional lethal effects have been postulated, including the alteration of a given target protein to produce lethal products.[25] For instance, protein synthesis disruption in the presence of aminoglycosides leads to the formation of toxic peptides that destabilize/permeabilize the inner membrane.[26] Similarly, the effect of macrolide antibiotics appears to be based on context-specific inhibition of peptide bond synthesis.[27] β-Lactams and teixobactin have been found to induce cell wall autolysis,[28,29] and fluoroquinolones appear to convert gyrases into endonucleases by forming a covalent gyrase–DNA cleavage complex.[30]

Acquired and intrinsic mechanisms of antibiotic resistance

Depending on the initial state of a given bacterial target, the inhibitory effect of antimicrobial agents can be counteracted by different intrinsic or acquired mechanisms of resistance that prevent antimicrobial compounds from binding to their targets. Enzymatic inactivation of antibiotics, for example, is a resistance mechanism typically acquired by horizontal gene transfer. Examples include aminoglycosides that can be inactivated by (substrate-specific) modifying enzymes, including acetyltransferases, phosphotransferases, and nucleotidyltransferases;[31,32] and β-lactam antibiotics that can be hydrolyzed by β-lactamases; the latter enzymes, in turn, can be inhibited by clavulanic acid. This is why a combination of both β-lactams and clavulanic acid is often used for treatment (Fig. 1).[33] Alternatively, antibiotic drug targets can be protected by additional factors or altered in a way that prevents inhibitors from binding.[32] Target site alterations can be achieved by covalent modifications, by the expression of alternative subunits, or by mutagenesis.[34] For example, bacterial DNA gyrases or DNA-dependent RNA polymerases become insensitive to antibiotics by one of a number of different point mutations (single-site alterations).[35,36] Other fluoroquinolone resistance mechanisms result from the production of protecting Qnr proteins or acyltransferases that are effective against CIP and norfloxacin, as well as efflux pumps.[37]

Under laboratory conditions, chloramphenicol- and doxorubicin (DOX)-sensitive *E. coli* have been shown to acquire multiple mutations when cultured continuously under increasing concentrations of drugs. These mutations are often located in either the gene *acrB*, which encodes the multidrug efflux pump (MDEP) AcrB, or the promotor region of the gene encoding the MdfA (*cmr*) efflux pump, as well as in genes encoding the regulatory proteins for their expression (*marR*, *acrR*, and *pcmr*).[38] Non-genetic causes, such as alternative physiological states within a bacterial population, give rise to intrinsic antibiotic persistence. Persisters manage to evade the toxic consequences of antimicrobials possibly because of their reduced biosynthetic activity. Dormant pathogens are hard to eliminate and are considered to be associated with diverse latent microbial infections.[25] Furthermore, dormancy in *E. coli* has been also shown to be associated with a higher expression of various MDEP components (*tolC, acrA*, *acrB, acrD, emrA, emrB, macA,* and *macB*), which contribute substantially to the intrinsic resistance of Gram-negative bacteria.[39] The difference between resistance, persistence, tolerance, and other phenomena, such as heteroresistance, and how to measure these properties within a bacterial population have been summarized and discussed recently.[40]

The intrinsic resistance of Gram-negative bacteria

MDEPs transport antimicrobial agents from the bacterial interior back to the environment. By reducing intracellular antimicrobial concentrations, they contribute to the intrinsic resistance of Gram-negative bacteria and support acquisition of other modes of resistance.[41] The efflux pumps of the Gram-negative bacterial subdivision are organized into a complex network with a mode of operation that is defined by Gram-negative morphology comprising two membranes, the inner and outer membranes.

Gram negatives—a two-membrane system reduces toxin permeation

In contrast to Gram-positive bacteria, which contain only an inner membrane and a much thicker cell wall, Gram-negative bacteria are surrounded by an additional outer membrane. The inner and outer membranes enclose the periplasm, an additional compartment next to the cytoplasm. Importantly, unlike the inner membrane, the outer membrane is highly asymmetric. While the inner leaflet consists of phospholipids, the outer membrane outer leaflet comprises lipopolysaccharide (LPS) (Fig. 1). The LPS molecules form, on the one hand, a hydrophilic permeability barrier at the bacterial surface,[7] while the acyl chains of the LPS in the outer leaflet—in conjunction with the inner leaflet phospholipids—constitute a hydrophobic permeability barrier. The outer membrane is interspersed with porins to allow an exchange of substances with the environment (e.g., in order to absorb nutrients or facilitate exchange of ions). Porins contain a certain degree of selectivity (with reference to size and polarity) and facilitate transport of molecules between the environment and periplasm.[42]

Altogether, the properties of the outer membrane favor the uptake of small, hydrophilic molecules over larger and more hydrophobic compounds. Most antimicrobials (see Fig. S1, online only), however, rather fall into the latter category. Diverse studies indicate that porins are involved in the uptake of various antibiotics. Antimicrobial drug resistance can be increased by porin gene expression downregulation or changes in the porin population composition, further reducing the permeability of the outer membrane.[42] Those antibiotics not directed against periplasmic targets must overcome the inner membrane as well to reach their targets in the cytoplasm (Fig. 1).

MDEPs from different transporter superfamilies counteract the influx of antimicrobials

The Gram-negative bacterial inner membrane, which separates the cytoplasm from the periplasm, is a distinct hydrophobic barrier with strongly regulated mechanisms of exchange. The presence of ion gradients (including the membrane potential) and the cytoplasm as source of chemical/redox energy enables active transport across this physical barrier.[43] Accordingly, the inner membrane contains the active components of MDEPs that either are secondary active antiporters driven by the proton motive force (PMF) or the electrochemical gradient of Na^+ ions, or are primary active exporters driven by ATP binding and hydrolysis.[44] Efflux pumps counteract the passive influx of their substrates along the concentration gradient by transporting them, in case of the single-component transporters, from the cytosol to the periplasm, or as part of a two-membrane-spanning tripartite complex from the periplasm across the outer membrane.[45–47] Of note, it is important to emphasize that efflux pumps that transport toxic compounds across the outer membrane are heavily dependent on the permeability of the latter.

The efficiency of tripartite efflux pumps to confer resistance relies on the physicochemical properties of the transported compound not only related to its affinity toward the efflux pump, but also by its ability to cross the outer membrane. The composition of the latter (including different types of porins), which is different among Gram-negative bacteria, determines the rate of influx and hence the concentration in the periplasm or inner membrane.

This important concept has been addressed recently and summarized in a review by Zgurskaya and Rybenkov.[48] In this sense, resistance against the accumulation of the drugs in the cell is counteracted by the synergism of efflux pump(s) and the outer membrane. By establishing the equilibrium between influx and efflux, the concentration of antimicrobial substrates in the cytoplasm and periplasm is kept low, allowing MDEPs to contribute essentially to the intrinsic drug resistance of Gram-negative bacteria.[49] Known bacterial MDEPs belong to a total of six different transporter families, which are the ATP-binding cassette (ABC) superfamily, the small multidrug resistance (SMR) family, the major facilitator superfamily (MFS), the multidrug and toxin extrusion (MATE) family, the resistance–nodulation–cell division (RND) superfamily, and the proteobacterial antimicrobial compound efflux (PACE) family.[50] These will be briefly introduced below. Structures of representative transporters of each (super)family have been included in Figure 1, as indicated.

Ann. N.Y. Acad. Sci. 1459 (2020) 38–68 © 2019 The Authors. *Annals of the New York Academy of Sciences* published by Wiley Periodicals, Inc. on behalf of The New York Academy of Sciences.

The ABC family

Members of the ABC superfamily are either homodimeric or (pseudo)heterodimeric ATP-driven transporters that are involved in the import and/or export of solutes. Each ABC transporter can structurally be subdivided into a transmembrane domain (TMD), which contains the substrate binding pocket, and two nucleotide-binding domains (which can be encoded by separate genes), responsible for ATP binding and hydrolysis.[51] In Gram-negative bacteria, ABC transporter efflux pumps can be either single-component transporters or part of a tripartite complex. The *Thermus thermophilus* ABC transporter efflux TmrAB, whose X-ray structure was solved at 2.7 Å resolution (PDB: 5MKK)[52] and predicted to function as a single (heterodimeric) component transporter, was shown to transport the antimicrobial dye Hoechst 33342 (HOE).[53] Recently, in the case of MacAB–TolC, a structural model of an assembled tripartite ABC transporter was, for the first time, obtained via single-particle cryo-EM at 3.3 Å resolution (PDB: 5NIK)[54] (see Fig. 1).

The families of SMR and PACE transporters

Transporters of the SMR family were shown to form parallel or antiparallel homo- or heterodimers with identical inward- and outward-facing states consisting of only four transmembrane (TM) helices in each subunit.[55,56] An optimized structure of the SMR family member EmrE (i.e., the apo-structure and in complex with various substrates, including inhibitory peptide compounds) from *E. coli* was obtained by microsecond-long molecular dynamic (MD) simulations[57] on the basis of a low-resolution X-ray structure (at 3.8 Å resolution) in complex with tetraphenylphosphonium (TPP) (PDB: 4B5D).[58] The transporter was shown to confer resistance against acriflavine, ethidium (ETH), methylviologen, and benzalkonium (BEN),[46,59] as well as aminoglycosides.[60] Conformational dynamics of SMR transporters appear to be modulated in an allosteric fashion by protonation.[61] Homologs of the *Acinetobacter baumannii* AceI MDEP, which confer resistance against synthetic bactericidal agents, such as chlorhexidine, ACR, proflavine, and BEN, have been suggested to form the new PACE family of transporters.[50] Size and predicted secondary structure of these transporters, which are not found in *E. coli*, appear to be similar to SMR family-type transporters.[44]

The major facilitator superfamily

The members of the extremely diverse MFS that are involved in multidrug efflux belong to the drug/proton (H^+) antiporter families 1 and 2 (DHA1/2), which differ in their substrate/proton stoichiometry. *E. coli* MdfA, a member of the DHA1 family, exports neutral or monovalent cationic compounds in exchange for a single proton.[62] MdfA substrates include CAT, tetracycline, norfloxacin, DOX, trimethoprim, ACR, ETH, and TPP.[62,63] An X-ray structure of MdfA with CAT bound to the central cavity of the transporter was solved at 2.5 Å (PDB: 4ZOW) in an inward-facing conformation.[64] Each MdfA single-component transporter is formed by two interconnected bundles of six TM helices, which were suggested to cooperate in an alternating access mechanism with ordered binding and release of proton and substrate.[62]

The MATE family

Bacterial MATE transporters can be divided into the NorM and DinF subfamilies of 12 TM drug/Na^+ or drug/H^+ antiporters (xenobiotic-transporting eukaryotic MATE transporters are described in Miyauchi *et al.*[65]). MDEPs of this family transport polyaromatic and cationic compounds, such as rhodamine 6G (R6G), ETH, and TPP.[44,66] Structures of Na^+-dependent NorM subfamily transporters have been solved by X-ray crystallography at 3.6 Å resolution in cation- and substrate-bound states.[67,68] The X-ray structure of the single-component *Bacillus halodurans* DinF (DinF-BH) transporter of the DinF subfamily, in which R6G was bound to the central cavity via mostly hydrophobic interactions, was solved at 3.7 Å resolution (PDB: 4LZ9).[68] For the drug/proton antiporter, an alternating access mechanism with ordered binding and release of proton and substrate was proposed, similar to MFS transporters described above. However, MATE and MFS transporters have different topologies in their pseudo-symmetrical 6 TM helix bundles.[44]

The RND superfamily

Members of the RND superfamily are present in all domains of life. RND-type transporters are involved

BOX 1. Diversity of RND-type transporters

As suggested by the terms *resistance, nodulation*, and *cell division*, RND transporters are involved in versatile cellular processes. On the basis of phylogenetic analysis, RND members are divided into a number of families[76] (www.tcdb.org). Members of the hydrophobe/amphiphile efflux 1 (HAE-1) and the heavy metal efflux (HME) families of Gram-negative bacteria transport and thereby confer resistance against diverse antibiotics and heavy metals, respectively. RND transporters of the Gram-positive HAE-2 and the Gram-negative HAE-3 subfamilies participate indirectly in resistance by transporting factors that contribute to the robustness of the cell wall (HAE-2)[69] or the outer membrane (HAE-3).[77] Members of the nodulation factor exporter (NFE) family have been suggested to export nodulation factors in order to stimulate the growth of root nodules as a (symbiotic) bacterial habitat.[69] With regard to cell division, Ptch1, a member of the dispatched family, was shown to bind the protein hedgehog, an important signaling factor in embryonic development and carcinogenesis.[78–81] In addition, members of the SecDF subfamily are involved in bacterial (and archaeal) protein translocation, where they act as membrane-integrated chaperons;[82] members of the eukaryotic sterol transporter (EST) family, such as the Niemann–Pick type C protein 1 (NPC1), play important roles in eukaryotic cholesterol homeostasis.[83] The diversity of RND transporters is also reflected in their oligomeric states. While members of the HAE-1 subfamily seem to exclusively form (homo)trimers,[69] the hopanoid transporter HpnN from *Burkholderia multivorans*, a member of the HAE-3 family, was found to form homodimers.[84] The SecDF protein of *Thermus thermophilus*[82] acts as a 12 TM heterodimer; and human NPC1,[85] as well as Patched, appears to be active as single RND subunits. Recently, the monomeric *Mycobacterium tuberculosis* RND mycolic acid/phosphatidylethanolamine transporter MmpL3 structure was solved.[86,87] The *E. coli* genome contains a total of 10 RND transporters (www.membranetransport.org). Characterized members are AcrB, AcrD, AcrF, MdtF, and the heterotrimeric MdtBC, all of which belong to the HAE-1 family, and the copper(I)/silver(I) transporter CusA, representing a member of the HME family. The heterodimeric protein-transporting SecDF belongs to its own family of transporters[82] (www.tcdb.org). The trimeric RND proteins from *E. coli* assemble into elongated tripartite complexes with six copies of a membrane fusion protein (MFP) and the homotrimeric outer membrane factors (OMFs) TolC or CusC.[88]

in many different cellular processes as summarized in Box 1. All RND-type transporters show high structural similarity in their TMDs, which in general contain 12 TM helices (sometimes, by lateral extensions, 13 or 14 TMs). The TMDs are arranged in two pseudo-symmetric 6 TM bundles, each containing a large external loop between TM1 and TM2, as well as between TM7 and TM8. Those loops, which usually form a large soluble domain, can be very different in size and shape.[69] Also, the oligomeric state is different between members of the subfamilies (see Box 1). The TMDs of well-studied representatives contain a proton relay network that directs protons along the electrochemical gradient across the membrane, driving conformational changes in both TM and soluble domains.[69–71] Most RNDs appear to be PMF-driven antiporters; however, VexF from *Vibrio cholerae* has been shown to be dependent on the presence of Na^+.[72]

In Gram-negative bacteria, RND transporters of the hydrophobe/amphiphile efflux 1 (HAE-1) family contribute (essentially) to the intrinsic resistance toward antibiotics. In contrast to all other families of efflux pumps, the characterized HAE-1 (and heavy metal efflux) family members are only active (i.e., confer resistance) in conjunction with membrane fusion proteins (MFPs) and an outer membrane factor (OMF), with which they form elongated tripartite complexes.[44,69] For the AcrAB(Z)–TolC tripartite complex from *E. coli*, structural models of up to 5.9 Å resolution (PDB: 5O66) were elucidated on the basis of single-particle cryo-EM data[73] (see Figs. 1 and 2). It has been shown that the inner membrane components, for example, AcrB and AcrD, from *E. coli* interact with the same MFP (i.e., AcrA) and OMP (TolC). The latter outer membrane channel shows even a higher promiscuity, since it can partner with several MFPs and is integrated in various tripartite systems, such as RND-type AcrAB–TolC, AcrAD–TolC, AcrEF–TolC, but also with ABC-type transporters, like MacAB and HlyBD, as well as with EmrAB, a member of the MFS. It was demonstrated that the substrate specificity of the entire tripartite RND complexes is (predominantly) determined by the periplasmic loops of the RND inner membrane protein (IMP).[74,75]

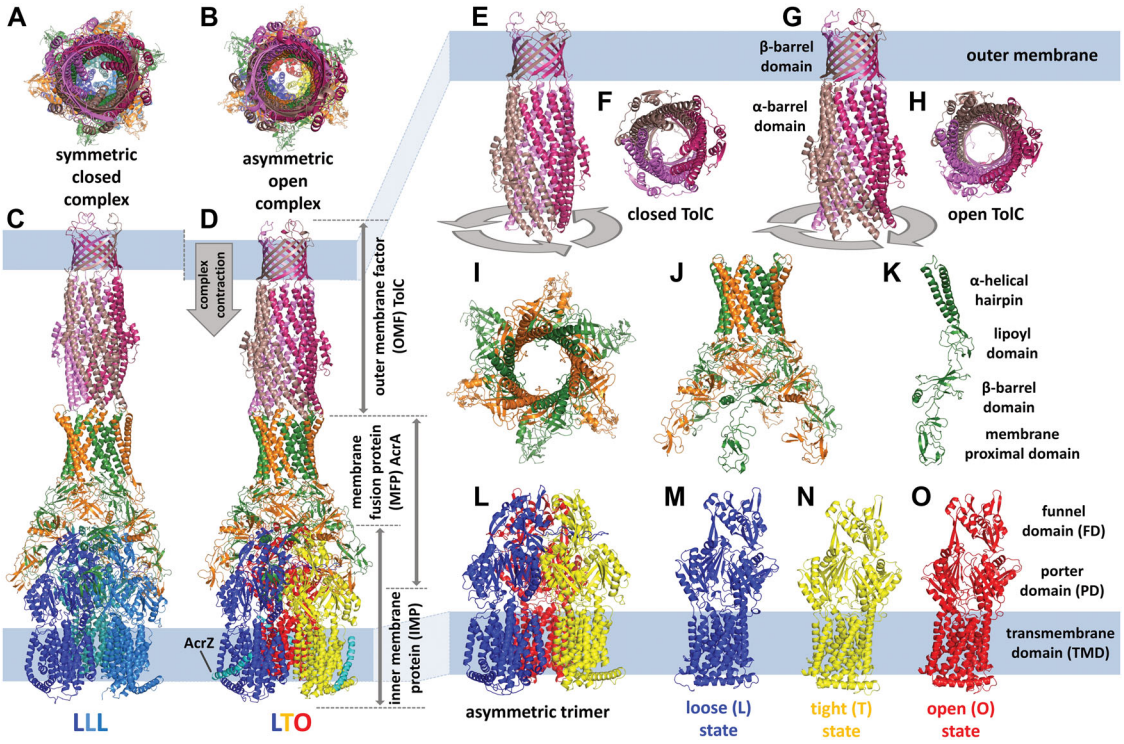

Figure 2. The AcrAB(Z)–TolC multidrug efflux pump complex. The structure of the AcrAB(Z)–TolC complex was solved via single-particle cryo-EM in essentially two different states: a symmetrically closed (LLL) resting (A, C) state and an asymmetrically open, active state (LTO) (B, D) (PDB: 5V5S and 5O66[73]). The structures were solved at 6.5 and 5.9 Å resolution, respectively. AcrB, the inner membrane protein (IMP) of the resistance nodulation and cell division (RND) superfamily forms a homotrimer (subfigure L), where the protomers can adopt the different conformational states: loose (subfigure M), tight (subfigure N), and open (subfigure O). AcrB can be structurally subdivided into three main domains, namely, a funnel (FD), a porter (PD), and a transmembrane domain (TMD) (O). The AcrB trimer is the core component of the tripartite complex that recognizes substrates and transduces the energy (proton motive force, PMF) into translocation of substrates. In the complex, the AcrB trimer is associated with six copies of the membrane fusion protein (MFP) AcrA, that form a membrane fused tubular structure inside the periplasmic space (I, J). The AcrA α-hairpins and lipoyl domains are organized in two rings above the AcrB trimer, while the β-barrel and membrane proximal domains (K) laterally interact with the core complex (C, D). The AcrA hexameric ring on the other side interacts via its α-hairpins with the outer membrane factor (OMF) TolC, establishing tip-to-tip interactions between the respective TolC α-barrel helices (C, D). TolC forms a homotrimer, where the β-barrel domain (G) creates a pore in the outer membrane. In a noncomplexed state, the TolC α-barrel domain (G) closes the pore toward the periplasm. Depending on the conformational state of the AcrB core complex, TolC was either found in a closed (when trimeric AcrB adopts the LLL state) (E, F) or an open conformation (when trimeric AcrB adopts the LTO state) (G, H) within the tripartite complex (C, D). The asymmetry is presumably induced by substrate binding, in a process not yet understood in detail, and causes the iris-like opening of the TolC α-barrel (G, H). The active asymmetric complex forms a continuous channel from the (closed) binding pocket of the O protomer (see Fig. 3) to the extracellular environment. During activation (TolC closed to open), the entire tripartite complex contracts by approximately 10 Å along the vertical axis compared with the symmetric resting state.

The AcrAB–TolC tripartite efflux machinery as the central element of a transporter network

Tripartite efflux pumps traverse the Gram-negative inner and the outer bacterial membrane with their IMPs and OMFs connected via their MFPs. In *E. coli*, the OMF TolC is shared by all tripartite RND efflux pumps of the HAE-1 family.[88] The constitutively expressed *acrAB–tolC* MDEP genes encode a machinery that contains three copies of the RND IMP AcrB, six copies of the MFP AcrA, and three copies of the OMF TolC[89] (see Figs. 1 and 2). When bacterial strains with deletions in several putative multidrug efflux genes were tested against different antimicrobial compounds, strains with deletions of

the genes encoding components of the AcrAB–TolC MDEP (e.g., Δ*tolC* or Δ*acrB*) were heavily impaired in conferring resistance toward the drugs.[90,91] The importance of the intrinsic resistance toward multiple compounds conferred by this transporter system is well documented by the systematic analysis of the *E. coli* KEIO collection[92] grown under various stress conditions.[91] Transporters from the MFS and ABC superfamilies involved in tripartite systems appear to play only a minor role in antimicrobial resistance, since their genes are not expressed owing to stronger regulation, as is the case, for example, for the *acrEF* RND-type genes.[59] In addition, many tripartite systems confer only resistance toward a small number of drugs, as shown for the tripartite MFS pump EmrAB–TolC or the tripartite ABC transporter MacAB–TolC.[59,93] This might also be due to the cognate function of the latter systems; for example, EmrAB contributes to the efflux of free fatty acids,[94] whereas MacAB is involved in the secretion of protoporphyrin[95] and enterotoxin II,[96] and is suggested to transport LPS.[97]

As demonstrated by many comprehensive studies,[59,90,91,98–100] the AcrAB–TolC MDEP confers (high level) resistance against a broad range of antimicrobial compounds, which are diverse in structure and size (structural formulas for some of these compounds have been compiled in Fig. S1, online only). These include different classes of antibiotics, such as macrolides, β-lactams, aminocoumarins, rifamycins, quinolones, oxazolidones, and tetracyclines, but also coloring agents, anticancer drugs, detergents, bile salts, and solvents. Apart from their differences, compounds recognized by AcrB have in common that they contain certain hydrophobic moieties.[70] More hydrophilic compounds, such as bi-anionic β-lactams (e.g., carbenicillin) and aminoglycosides (e.g., KAN) are not, or are poorly, transported by the AcrAB-TolC pump, but much better by the closely related AcrAD–TolC MDEP.[101–104] Whenever *acrD* expression is induced by environmental stimuli,[105] it can close this functional gap of the AcrAB–TolC system.

The broad substrate spectrum of AcrB corresponds to the sum of substrates transported by the diverse single-component MDEPs of the ABC, MFS, MATE, and SMR (super)families (in addition to those substrates with periplasmic targets, e.g., β-lactams). The individual single-component transporters each appears to recognize only a limited number of substrates.[59] However, a certain degree of redundancy is apparent, as some substrates are transported by more than one single-component transporter across the inner membrane.[46,59] This might be one reason why cells with individual chromosomal deletions of single-component transporter genes in most cases do not show higher susceptibility.[90] Single-component efflux pumps transport compounds across the inner membrane, while tripartite RND complexes, such as AcrAB–TolC or the homologous MexAB–OprM complex from *P. aeruginosa,* appear to mediate transport across the outer membrane as has been implied from *in vivo*[106] and *in vitro*[107] experiments.

Despite the fact that RND MDEPs span the inner bacterial membrane, they at least "prefer" to capture their substrates from the periplasm.[108] However, if bacterial cells lack all single-component transporter genes responsible for the efflux for a certain toxin across the inner membrane, sensitivity similar to bacteria lacking *acrB* is observed.[45–47] Clearly, if the single-component transporters are not present, the AcrAB–TolC system appears incapable of conferring resistance. These results might be interpreted as that the single-component transporters accumulate the drugs at the periplasmic side, in the outer leaflet of the inner membrane. If true, the increased drug concentration in the outer leaflet will be beneficial for the rate of drug transport by the AcrB component. Drugs with a high flip-flop rate equilibrate fast over both leaflets of the inner membrane, thereby decreasing the efficiency of binding and transport by AcrB. In addition, rapid equilibration with the cytoplasmic concentration (e.g., in the case of ETH) ultimately causes intoxication by the incoming drug. Single-component transporters shift this equilibrium toward the outer leaflet of the inner membrane and hence increase the drug concentration according to thermodynamics, depending on the number of protons coupled per drug. This hypothesis assumes that AcrB can only capture drugs from the outer leaflet of the inner membrane or from the periplasm. Structural features of the pump that support this assumption are described below.

Accordingly, drug efflux from the cytoplasm across the outer membrane, as illustrated in Figure 1, appears to be a two-stage process in which substrates are first transferred by various single-component transporters to the periplasm,

from where they are sequestered and transported across the outer membrane by AcrAB–TolC.[46] The fact that the latter step is only catalyzed by AcrAB–TolC for these substrates (see Fig. S1, online only) illustrates the importance of this complex pump machinery as the central element of the efflux network.

Tripartite RND efflux pumps from a clinical perspective

RND MDEPs, such as AcrAB–TolC from *E. coli* and *Salmonella enterica*, MexAB–OprM from *P. aeruginosa*, CmeABC from *Campylobacter jejuni,* and AdeABC from *A. baumannii,* are often upregulated in clinical isolates.[109,110] In addition, RNDs have been found encoded on mobile genetic elements,[108] conferring for instance nitrofurantoin resistance (by OqxAB) to uropathogenic *E. coli*.[111,112] The activity of MDEPs is also expected to support the acquisition of additional mechanisms of resistance[41,113,114] by reducing intracellular drug concentrations to sublethal levels that are supposed to enhance the genome-wide mutation rate.[115]

The outer membrane, as the front defense line and essential part of the integral framework of tripartite efflux in Gram-negative bacteria, is a target of diverse peptide antibiotics, such as the cyclic polycationic polymyxins. Currently, polymyxins, which disrupt the outer membranes and kill bacteria by permeabilizing their inner membranes[116] (Fig. 1), are the strongest weapon in the fight against otherwise resistant Enterobacteriaceae. However, their efficiency appears to be impeded more and more by acquired resistance.[117,118] Not surprisingly, carbapenem-resistant *A. baumannii*, *P. aeruginosa* strains, and carbapenem and third-generation cephalosporin-resistant Enterobacteriaceae, including *Klebsiella pneumoniae*, *Escherichia coli*, *Enterobacter* spp., *Serratia* spp., *Proteus* spp., and *Providencia* spp., *Morganella* spp. (all Gram-negative organisms), were given top priority by the World Health Organization in the search for new antimicrobial agents.[117]

The primary defense mechanisms of Gram-negative bacteria, which are based on a pronounced diffusion barrier with opposing selective properties (hydrophilic/hydrophobic), additional compartmentalization (periplasm/cytoplasm), and a multifunctional efflux machinery, complicate the development of new active substances that would ideally be well penetrating.[108] Alternatively, there are different approaches, such as making use of existing antimicrobials in combination with efflux pump inhibitors.[119–121] This challenging approach requires a more detailed understanding of the molecular binding and transport mechanisms of tripartite RND efflux pumps.

Structural properties and dynamics of the AcrAB(Z)–TolC complex

A first imaging method–derived structural model for the AcrAB(Z)–TolC tripartite complex was determined by Du *et al.* using single-particle cryo-EM.[89] The low-resolution structure (16 Å) gave a first impression of the structural organization of the elongated tripartite complex comprising homotrimeric OMF TolC, six copies of the MFP AcrA, the homotrimeric IMP AcrB, and three copies of the small single TM helix protein AcrZ. Further optimization of the experimental conditions led to the symmetrical (LLL) and asymmetrical (LTO) complex models at 6.5 Å (PDB: 5V5S) and 5.9 Å resolution (PDB: 5O66),[73] which provided more detailed insights into the interactions of the individual complex components, as described below (see Fig. 2). As these complexes were obtained by genetically engineered AcrA/AcrB fusions, it was important that Daury *et al.* (by negative-stain EM) showed that native AcrAB–TolC and MexAB–OprM complexes in nanodiscs appeared to have the same architecture.[122] Just recently, Tsutsumi *et al.* solved the MexAB–OprM structure at 3.6–3.8 Å resolution by single-particle cryo-EM.[123] Of note, the structure and, in particular, the interactions between MexA and OprM had been correctly predicted earlier by López *et al.* using sequence covariation analysis and microsecond-long MD simulations.[124] This and other successful predictive MD simulations used in the field of efflux pumps[125–133] emphasize that the predictive quality has been improving over the years, and will be an additional important asset in deciphering the structure/function relationship of efflux pumps.

Acriflavine resistance protein B

The first crystallographic structure of the 1049 AA (113.6 kDa) acriflavine resistance protein B (AcrB) from *E. coli* was solved at 3.5 Å resolution by Murakami *et al.* as a symmetrical (LLL) trimer,[134] a conformation that was later proposed

to represent the unoccupied resting state of the transporter.[135] Asymmetric (LTO) structures of AcrB were obtained under different crystallization conditions,[136,137] which also included the use of designed ankyrin repeat proteins (DARPins) as crystallization chaperones.[138] With the help of the latter, resolutions up to 1.9 Å (PDB: 4DX5) could be achieved.[139] In the asymmetric AcrB trimer, which appears to resemble the active state of AcrB, each protomer has a different conformation. The individual conformations were suggested to represent defined states of a transport cycle, which will be further discussed below.

According to their anticipated roles in the functional rotation—which are the (1) access of substrates, (2) their binding, and (3) their extrusion—the individual conformational states were named *access*, *binding,* and *extrusion*,[136] or, alternatively, in analogy to the F_1F_o-ATP functional rotation,[140] *loose* (L), *tight* (T), and *open* (O).[137,141] In the figures shown throughout this review, unless indicated, colors are assigned to the individual conformational states of AcrB: blue (L), yellow (T), and red (O). Under crystallization conditions resulting in asymmetric AcrB trimers, several AcrB/substrate costructures were obtained in which substrate molecules were bound within one trimer to binding pockets of the L, T, or even to both L and T protomers.[136,139,142,143] AcrB can be structurally divided into a funnel domain (FD, or docking domain) important for AcrB trimerization,[144,145] a TMD responsible for the energy transduction to facilitate drug transport, and the porter domain (PD) that contains the binding pockets (proximal and distal, or access and deep binding pockets (DBPs)) and mediates substrate uptake, recognition, and translocation.

Acriflavine resistance protein Z

AcrB was found to stably interact with the small 49 amino acid (AA)–long (5.3 kDa) inner membrane acriflavine resistance protein Z (AcrZ), whose expression is coregulated with *acrAB*.[146] AcrZ essentially consists of a single tilted helix inside the membrane and thereby fits into a wide groove in the AcrB TMD.[73] The deletion of this small accessory protein led to a moderate reduction in activity with respect to some AcrB substrates.[91,146] Single TM proteins, such as AcrZ and YajC, shown to interact with AcrB,[73,146,147] appear to be present in some Enterobacteriaceae, and might function as allosteric modulators of RND MDEPs.[73]

Acriflavine resistance protein A

The 42.2 kDa (397 AAs) periplasmic MFP acriflavine resistance protein A (AcrA) is produced as a precursor protein containing an N-terminal signal helix (residues 1–24). The mature protein, which lacks this signal peptide, is anchored to the inner membrane via palmitoylation (lipid anchoring) at Cys25.[148] MexA, an AcrA homolog from *P. aeruginosa*, has been experimentally shown to be palmitoylated[149] and was the first MFP for which the X-ray structure was solved at 2.4 Å. The structure revealed an elongated architecture formed by a membrane proximal (MP) domain, a β-barrel domain, a lipoyl domain, and an α-helical hairpin motif.[150,151] Shortly thereafter, the AcrA structure was published showing an identical architecture,[152] and, on the basis of a refined MexA structure, the thus-far elusive MP domain of AcrA was revealed.[153] In the latter study, comprehensive cross-linking studies with AcrA/AcrB (based on the refined MexA structure) led to the first insights into the AcrA/B interactions.

In the tripartite complex, as was shown from the first single-particle cryo-EM structures, AcrA forms a hexameric assembly[73,89] similar to the quaternary structure observed in crystals of MacA from *Actinobacillus actinomycetemcomitans.*[154] In the hexameric assembly, the AcrA hairpins, lipoyl, and β-barrel domains are densely packed, enclosing a central channel that merges at its lower end into the funnel on the upper side of the trimeric AcrB periplasmic domain. From the four AcrA subdomains, only the β-barrel and the MP domain are in direct contact to AcrB, whereby adjacent AcrA protomers differ in their interaction. Protomer I is in contact to the AcrB subdomains FC (or DC, C-terminal funnel or docking domain), PC1, and PC2 (C-terminal porter subdomains 1 and 2), while protomer II interacts with the FN (or DN, N-terminal funnel or docking domain) and PN2 (N-terminal porter subdomain 2) subdomains[73,89] (Figs. 2 and 3). The interaction of protomer II significantly differs from the interaction that was observed in the CusAB (Cu^+/Ag^+ RND/MFP antiporter) complex structure,[155] which might be a preassembled state in the absence of the OMF (CusC). As has been shown for AcrAB(Z)–TolC[73,156] and MacAB–TolC

Ann. N.Y. Acad. Sci. 1459 (2020) 38–68 © 2019 The Authors. *Annals of the New York Academy of Sciences* published by Wiley Periodicals, Inc. on behalf of The New York Academy of Sciences.

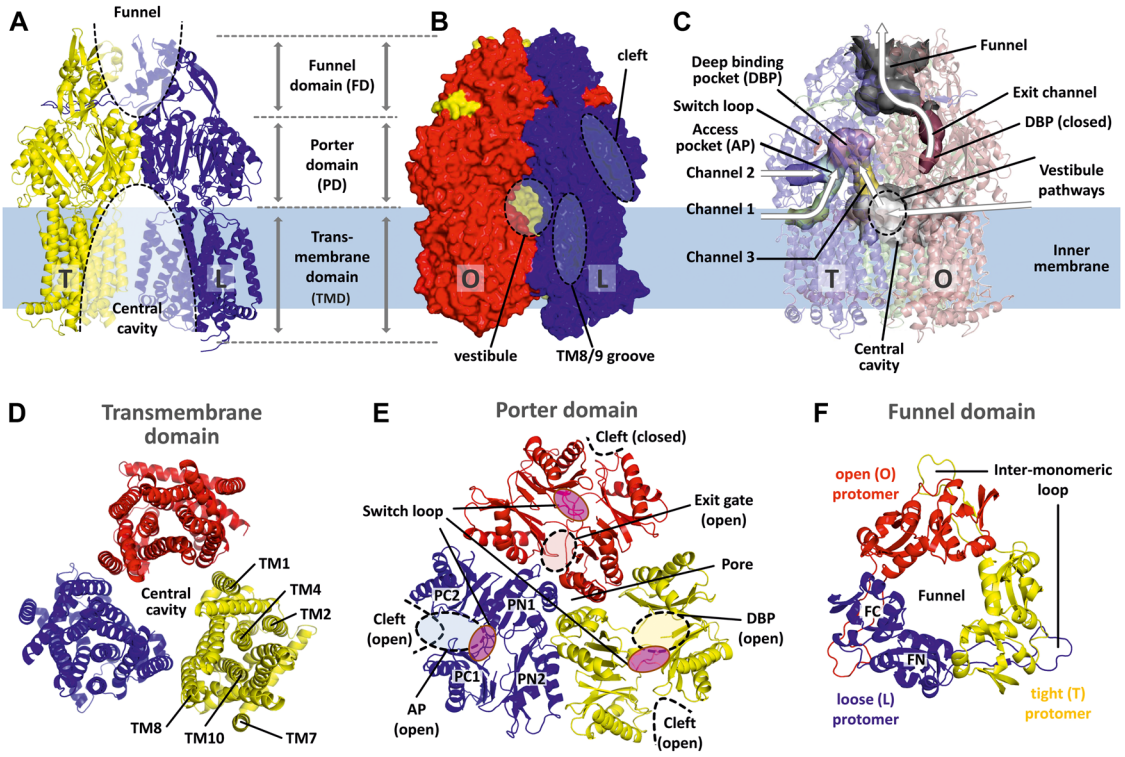

Figure 3. Architecture of the RND core component—the AcrB inner membrane protein. The AcrB protomers of the asymmetric trimer adopt different conformations (L, loose—blue, T, tight—yellow, and O, open—red). AcrB can be structurally subdivided into a funnel domain (FD), a porter domain (PD), and a transmembrane domain (TMD) (A), which are each shown from a top perspective in D, E, and F. The TMD consists of 12 transmembrane (TM) helices per protomer that are arranged in two pseudo-symmetric bundles. TM4 comprises titratable residues (D407 and D408) of the proton relay network involving TM4, TM10, and TM11 (residues D407, D408, K940, and R971). This relay is found two-thirds across the way through the membrane in each TMD. The three TMDs enclose the central lipid-filled cavity (A, D). The PD (and the FD) is formed by the two periplasmic loops between TM1 and TM2, as well as TM7 and TM8 (D). Each PD can be subdivided into two N- (PN1 and PN2) and two C-terminal subdomains (PC1 and PC2). The subdomains PC1 and PC2 form a cleft in the L and T conformation (B) and comprise the access pocket (AP) (E). The switch loop, which is part of the PC1 subdomain, separates the AP from the DBP present in the T protomer between PC1 and PN2. In the O conformation, the cleft, AP, and DBP are closed, but an exit tunnel between PN1 and PN2 subdomains is apparent (C). The PN1 subdomains form a pore in the center of the trimer, which is not solute accessible because of the tight packing (E). Trimerization is mainly mediated by the long intermonomeric loops, which are part of the FD. These loops and the FD remain mostly rigid during conformational cycling and can be seen as a scaffold during functional rotation (F). Figure 4 discusses the conformational transitions in the PD and TMD and their coupling in further detail. The asymmetric RND core component contains diverse substrate entry channels in the L and T conformation (C). Channel 1 (CH1) starting above the TM8/TM9 groove (B) is postulated to guide substrates from the outer leaflet of the inner membrane to the AP. The cleft pathway via CH2 also leads to the AP. Some compounds might also enter the central cavity via the vestibules between the protomer interfaces at the level of the membrane plane (B, C). CH3 was predicted to connect the central cavity directly to the DBP. All entry CHs are closed in the O protomer, while an exit channel connecting the exit gate to the funnel opens during the T to O transition. (Subfigure C was adapted from Fig. 6 in Neuberger *et al.*[164])

structures,[54] the MFPs (AcrA and MacA) bridge the periplasm and connect the IMP components to TolC via α-helical hairpin tip-to-tip interactions. In doing so, the substantially longer hairpin of MacA appears to compensate the smaller (shorter) periplasmic domain of MacB (Fig. 1).

The outer membrane factor TolC

In contrast to other Gram-negative bacteria, such as *P. aeruginosa*, which contain many different OMFs, enterobacteria, such as *E. coli,* essentially have only a single *tolC* gene. TolC is shared between many

different transporters covering different physiological processes, including the expulsion of metabolites, acid tolerance, cell membrane integrity, virulence, and antibiotic resistance.[157] TolC is synthesized as a 53.7 kDa (493 AAs) protein and cotranslationally exported into the periplasm, from where it is incorporated into the outer membrane, depending on the BamA/BamD complex.[158] As a homotrimer, TolC forms a 12-stranded β-barrel outer membrane pore domain whose opening merges into a 100 Å long α-barrel periplasmic domain that, in turn, consists of a total of 12 alternating continuous and pseudo-continuous α-helices (Fig. 2). TolC was crystallized at 2.1 Å resolution in a closed state in which the helices at the lower end of the α-barrel are twisted into each other like a closed iris diaphragm.[159] The closed state was shown to be stabilized by a network of intra- and intermonomer hydrogen bonds and salt bridges, whose disruption results in significantly higher ion conductivity,[160] and to structural characterization of (partially) opened states.[161,162] The presence of free (noncomplex associated) OMF in a closed state might prevent an uncontrolled exchange of (toxic) substances between the periplasm and the extracellular environment.

Structural and functional dynamics of the AcrAB(Z)–TolC complex

The structure of the apo (LLL) AcrAB–TolC complex (PDB: 5V5S)[73] and the low-resolution structures reported previously[89,163] were obtained from Cys-crosslinked or directly engineered protein fusions, which left the question open whether the complexes fully resemble the situation in the native tripartite efflux pump setup. Apo-complex formation was achieved with three of the six AcrA molecules Cys-crosslinked to AcrB, resulting in a structure at 6.5 Å. This tripartite setup was very similar, however, to structures of native AcrAB–TolC or MexAB–OprM complexes in nanodiscs.[122] In the apo-state, TolC was still in a closed conformation akin to that reported for the free protein,[159] and the AcrA protomers were only loosely packed without sealing the enclosed cavity toward the periplasm (Fig. 2). In the presence of substrate (e.g., puromycin (PUR)), however, the trimeric AcrB core complex adopted an asymmetric (LTO) conformation (PDB: 5O66).[73] Furthermore, the asymmetry in the AcrB trimer is associated with the repacking of the neighboring AcrA β-barrel and MP domains and in particular the reorientation of the α-helical coiled-coil hairpins, the flexibility of which was suggested important earlier on.[152] These reorientations, which involve all AcrA subdomains, lead to the iris-like opening of TolC and the sealing of the efflux channel toward the periplasm. Accordingly, the funnel of AcrB, from where the pumped substrates emerge from the AcrB O protomer, is in direct contact with the extracellular environment. In addition, the formation of an active pump system causes an axial compression of the entire complex by about 10 Å and the transition from a triple symmetry to a quasi-sixfold symmetrical interaction between AcrA and TolC.[73] In both AcrAB(Z)–TolC and the MacAB–TolC complexes, the opening of the OMF is associated with a tightly interlocked tip-to-tip interaction between the MFP hairpins and those of the TolC α-barrel domain.[54,73,124] However, these interactions involve only a few residues and are likely rather transient in order to rapidly close TolC and, presumably, prevent substrate reflux when AcrB is not actively pumping. In summary, the entire tripartite efflux pump appears to be a highly allosteric machinery in which conformational changes in the IMP are coupled to the OMF via the intermediate MFPs.[44,164]

Concerning tripartite complex dynamics, the homologous MexAB–OprM complex was reconstituted into a two-liposome system, and substrate transport was associated with a rapid PMF consumption[107] followed by a subsequent dissociation of the complex.[165] Considering these findings and the observation from Kralj *et al.* that in *E. coli* a rapidly spiking (∼1 Hz) PMF coincided with the efflux of the potential AcrB substrate tetramethyl rhodamine methylester,[166] we and others have suggested that the AcrAB–TolC MDEP operates in a discontinuous fashion.[167]

Some uncertainty still remains concerning the tripartite setup, since clear cross-linking between AcrB and TolC has been observed.[168] Moreover, the expression of genetic fusions between *acrA* and *acrB* in an *E. coli* Δ*acrAB* strain resulted in drug resistance. Since trimerization (and no higher oligomeric state) of AcrB has been established, the latter results imply that stoichiometric AcrA/AcrB (e.g., 1:1) is sufficient for pump activity, and immunoblot analysis indicated that no free AcrA (e.g., as result from proteolytic cleavage of

Ann. N.Y. Acad. Sci. 1459 (2020) 38–68 © 2019 The Authors. *Annals of the New York Academy of Sciences* published by Wiley Periodicals, Inc. on behalf of The New York Academy of Sciences.

the AcrA–AcrB fusion) is present. Nevertheless, some degradation or transcriptional/translational separation of the AcrA–AcrB fusion must have occurred, since "free" AcrB was observed in the same samples.[200]

Architecture of the RND core component—the AcrB inner membrane protein

The model of the asymmetric AcrB X-ray structure solved at 1.9 Å (PDB: 4DX5)[139] displays the homotrimeric core component of the AcrAB(Z)–TolC RND MDEP (Fig. 3). It can be structurally subdivided into an FD, a PD, and a TMD (Fig. S2, online only). The N-terminal (FN) and the C-terminal (FC) halves of the FD that constitute the funnel-like depression in the upper part of the periplasmic domain are involved in AcrB trimerization via a long intermonomeric loop, which penetrates the adjacent protomer.[144,169] Since the FDs of each protomer appear structurally identical between the different conformational states,[137] these are likely to form a scaffold for the conformational transitions occurring in the PD and TMD during the transport cycle.

The 36 TM helices containing TMD are more loosely packed and are enclosing a central cavity. This cavity is occupied with lipids forming a hexagonal arrangement[170] and suggested to be involved in the interprotomer conformational transduction. The TMD of each protomer is arranged in two pseudo-symmetric bundles (TM1–TM6 and TM7–TM12). Each of the TM bundles comprises a central TM helix (TM4 and TM10), which contains titratable residues of a proton relay network (AAs D407, D408, and K940). These residues and R971 on TM11 are involved in sequential protonation and deprotonation and are central to the energy conversion required for substrate transport. Accordingly, the TMD and PD, the latter formed by the two periplasmic loops between TM1 and TM2 as well as between TM7 and TM8, are conformationally coupled.[128] Each PD can be subdivided into two N-terminal and two C-terminal subdomains (PN1, PN2, PC1, and PC2). These subdomains act as rigid bodies adapting different relative orientations during the conformational cycling and constitute the structural differences between the individual conformers (L, T, and O) of the asymmetric structure. In the L and T conformation, the PC1 and PC2 subdomains form a vertical cleft toward the periplasm. The interspace between these subdomains also comprises the access pocket (AP). A further substrate pocket, the DBP, is composed of PN2 and PC1 (and PN1) subdomains, and is present in the T state only. Both pockets are separated from each other by an eleven amino acid long switch loop motif, a feature important for the transport of substrates (Fig. 3).

Computational structure analysis gave rise to diverse substrate entry channels in the L and T conformation of the asymmetric trimer. Channel 1 (CH1), which was observed in the TMD/PC2 interface of the T protomer above the TM8/TM9 groove,[138] appears to guide substrates from the outer leaflet of the inner membrane to the AP–DBP transition zone. The cleft pathway via CH2, observed about 15 Å above the putative membrane plane in both the L and T conformation, provides alternative access to the AP[136,137,139,142] (Fig. 3). Some compounds, as has been suggested from symmetrical (LLL) AcrB/substrate costructures,[171,172] might also enter the central cavity via the vestibules between the protomer interfaces. For planar aromatic cations, an alternative input channel (CH3) was predicted for the T protomer, which would establish a direct connection between the central cavity and the DBP bypassing the AP and the switch loop.[173] In the O conformation, the cleft, AP, DBP, and all entry channels are closed, but an exit tunnel/gate between PN1 and PN2 is present. The exit gate and the exit channel (CHe), exclusively open in the O state, connect the transporter's interior to the AcrB funnel and the AcrA/TolC exit duct of the tripartite complex that is in contact with the extracellular environment.

Remote alternative access drug/proton antiport in AcrB

The individual protomer conformations (L, T, and O) in the asymmetric structures of AcrB were interpreted as intermediate states of a transport cycle in which each protomer undergoes consecutive conformational changes.[136,137] In order to visualize the molecular processes within the PD (PN1, PN2, PC1, and PC2 subdomains) and the conformationally coupled TMD (TM1–12), individual protomers of the high-resolution 1.9 Å resolution structure (PDB: 4DX5)[139] were superimposed via their rigid FDs (PD) and TM4–6 (TMD), respectively, as

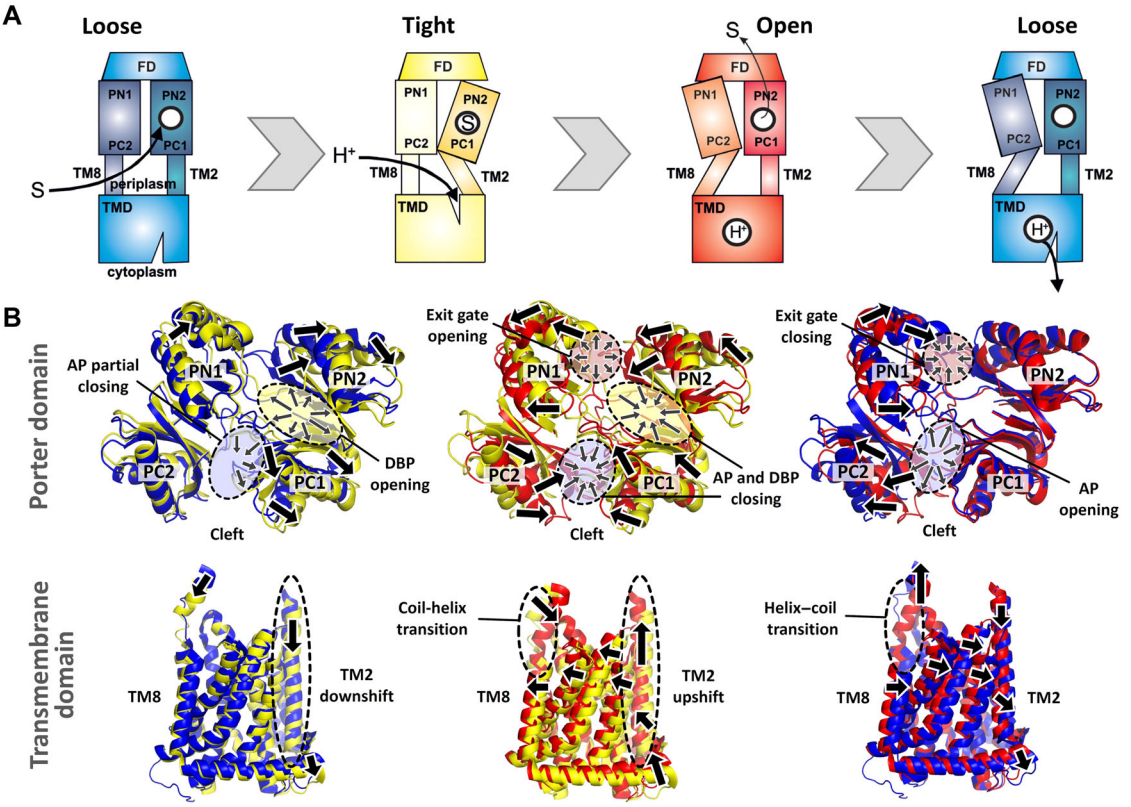

Figure 4. Remote alternative access drug–proton antiport in AcrB. The individual conformers (L, loose—blue, T, tight—yellow, and O, open—red) of the asymmetric AcrB trimer are considered as intermediate states of a transport cycle (illustrated in A), which each protomer undergoes sequentially. The processes in the porter domain, PD (with the N- and C-terminal subdomains PN1, PN2, PC1, and PC2, top view) and the transmembrane domain, TMD (with transmembrane helices TM1–12, side view) and the coupling between both are shown on a structural level in B. For this purpose, the consecutive states (L–T, T–O, and O–L) were superimposed. In detail, the PDs were superimposed using the funnel domain (FD) as a rigid scaffold, since this domain does not show larger conformational changes during the proposed functional rotation cycle. The individual TMDs were superimposed on TM4–6, also considered to be a rigid body scaffold during the cycle, in order to visualize the differences between the three states within the TMD. The coupling between the proton-translocating TMD and the substrate-translocating PD is mediated in particular by vertical shifting of TM2, which is directly linked to the PN2 subdomain. In the L protomer, the access pocket (AP) between PC1 and PC2 is open, while the deep binding pocket (DBP) between PC1 and PN2 subdomains is closed. Because of the L–T transition, both states are possibly present also in the absence of substrates, the subdomains PN2 and PC1 swing apart, causing the DBP to open and the AP to become smaller. The T state might then be stabilized by substrate binding in the DBP. The formation of the DBP and substrate binding is coupled to a downshift in TM2 and further smaller TM displacements making the TMD accessible for protons from the periplasmic side. The protonation of central titratable residues (D407 and D408) drives the T–O transition. Strong conformational changes within the TMD, including a TM2 upshift and a lateral movement of TM8, cause reorientation of all PD subdomains. The tilting of the PN1 subdomain opens the exit gate between the PN1 and PN2 subdomains through which substrates can be extruded as a consequence of DBP and AP closing. The proton release to the cytoplasm leads to a wide-reaching revision of the shifts within the TMD. However, the position of TM2 is hardly affected, which is presumably why conformational changes in the O to L transition in the PD are restricted to the subdomains PN1 and PC2. The opening of the cleft (AP) and the closing of the exit gate finally bring the system back to its initial L state. (Subfigure A was adapted from Fig. 3 in Müller *et al.*[167])

previously described[128,137] (Fig. 4). The coupling between the proton-translocating TMD and the substrate-translocating PD appears to be carried out by vertical shifts of TM2, which is directly connected to the PN2 subdomain, and the lateral movement of TM8 as consequence of the disengaged state of the TMD bundles. It has been recently suggested that the coil-to-helix and helix-to-coil transitions

in TM8, which is connected to the PC2 subdomain, are a consequence, rather than the cause, of interdomain coupling.[173] Nevertheless, the TM8 helix itself reacts to the protonation of the D407 and D408 residues, causing a lateral shift and, consequently, movement of the PC2 and PN1 subdomains (Fig. 4). Rearrangements in the hoisting loop (the region of TM8 where the coil-to-helix transition happens), also called the convertible TM-section, appear to be involved in the opening and closing of CH1.

Symmetrical LLL structures[73,134] and MD simulations[125] suggest that the L conformation is the preferred state in absence of substrates. Assuming that the L conformation is the starting point of a transport cycle, the AP between PC1 and PC2 subdomains will be open, while the DBP between PC1 and PN2 subdomains is closed. As a consequence of the L–T transition, the subdomains PN1 and PC1 swing apart, causing the DBP to open and the AP to become smaller. The binding of substrate molecules to the DBP stabilizes the T state, which is coupled to a downshift in TM2 and further, smaller TM displacements that make the TMD accessible for water molecules from the periplasmic side (Fig. 4). The formation of a water molecule network enables the protons to access the central titratable residues (D407 and D408) whose protonation drives the T–O transition.[128] Strong conformational changes within the TMD, such as a TM2 upshift, cause the reorientation of the PN1 and PC2 subdomains that did not move significantly during the L–T transition. The tilting of the PN1 subdomain in the direction of the adjacent protomer opens the exit gate between PN1 and PN2 subdomains through which substrates can be extruded toward the exit funnel as a consequence of the closure of the DBP and AP. Proton release to the cytoplasm leads to a wide-reaching revision of the shifts within the TMD. However, the position of TM2 is hardly affected, which is presumably why conformational changes in the PD during the O to L transition are restricted to PN1 and PC2 subdomains only. The opening of the cleft (AP) and the closing of the exit gate finally bring the system back to its initial L state (Fig. 4). Accordingly, the processes within the PD and TMD of each protomer can be considered as intermediates of two remote alternating access transport mechanisms.[128] As reversible Cys-crosslinking studies[174] and single-protomer exchange experiments[71] have shown, there is a mutual dependence not only within the subdomains of a protomer, but also between the individual protomers.

A single AcrB subunit with a critical mutation in the proton relay network (D407A) was sufficient to render the entire tripartite complex inactive.[71] Accordingly, the locking of a single subunit seems to prevent the others from completing their conformation cycle as well. These findings and the positive cooperativity observed in kinetic experiments with different penicillin antibiotics[175] support the bi-site activation hypothesis in analogy to the F_0F_1 ATPase, according to which the release of a substrate requires the binding of another substrate at a different binding site.[70] Different subprocesses were also suggested to take the advantage of each other when conformational transitions in the TMD were speculated to move FUS in an elevator-like mechanism from a membrane-associated state in the direction of a further potential entry site.[176] The heterotrimeric RND efflux pump $MdtB_2C$ might be considered as a special example of mutual dependence between individual protomers. While MdtC seems to be predominantly involved in substrate binding and transport, the MdtB components appear to translocate protons in order to provide the required energy.[177,178] Interestingly, for CmeB (an AcrB homolog from *C. jejuni*), it was proposed that individual protomers operate independently of each other.[179] However, the examination of the isolated IMP component might not necessarily resemble the conformational dynamics within the assembled tripartite complex.

Substrate recognition and inhibition of the AcrB RND core component

As elucidated by Nakashima *et al.*[142] and Eicher *et al.*,[139] the PDs of the asymmetric AcrB trimer harbor two large internal substrate (binding) pockets that are separated from each other by an 11-amino-acid–containing switch loop motif (residues 613–623) (Fig. 5). The AP and DBP are created by rigid body movements of the porter subdomains as elaborated above. In the L and T states, the PC1 and PC2 subdomains comprise the AP, while the DBP is formed by the PN2, PC1, (and PN1), exclusively in the T state. The boundaries of the pockets thus essentially consist of the rigid β-sheets of the subdomains, but also the more flexible loop sequences of the PC1–PC2 "connecting loop" (residues 666–679) at the bottom of the AP, the serine-rich "serine loop"

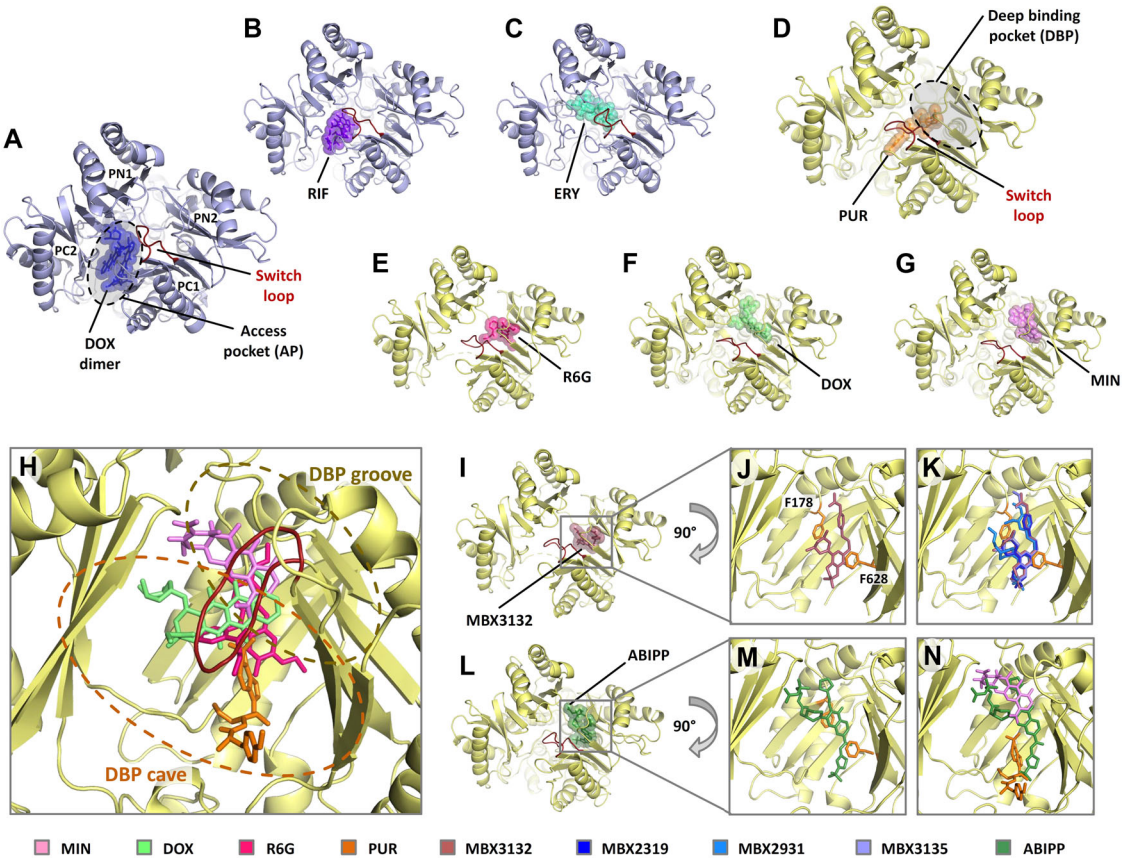

Figure 5. AcrB substrate and inhibitor costructures. The porter domains of substrate-bound L (loose, light blue) and T protomers (tight, pale yellow) from known asymmetric structures are shown from a top perspective with the substrate highlighted in a combined stick and sphere representation. A doxorubicin dimer (DOX dimer (blue) PDB: 4DX7) (A) and rifampicin (RIF (purple) PDB: 3AOB) (B) are located in the access pocket (AP) of the L protomer. The macrolide antibiotic erythromycin (ERY (cyan), PDB: 3AOC) (C) bound to the L state and the aminoacyl-tRNA analog puromycin (PUR (orange), PDB: 5NC5) (D) bound to the T state were found in an orientation interacting with residues of both the AP and deep binding pocket (DBP). Rhodamine 6G (R6G (pink), PDB: 5ENS) (E), monomeric doxorubicin (DOX (lime), PDB: 4DX7) (F), minocycline (MIN (violet), PDB: 4DX5) (G), as well as the inhibitory compounds ABIPP (forest green, PDB: 3W9H) (I) and MBX3132 (raspberry red, PDB: 5ENQ) (L), are localized in the DBP of the T protomer. The individual costructures can be considered as sequential intermediates along the substrate pathway from the outer AP to the inner DBP each representing a local energetic minimum for the interaction between AcrB and its ligand. The switch loop, indicated in dark red, contributes to the recognition in both pockets. The DBP can be subdivided into an upper groove, the narrow-elongated area of the DBP between the β-sheets of the PN2 and PC1 subdomains, and a lower more open cave, which is limited toward the lower side by the transmembane domain (TMD) (H). While MIN is bound to the groove and PUR is mainly bound in the cave, the inhibitors ABIPP (J) and MBX3132 (M) interact tightly with both DBP regions, including extensive π–π stacking interactions with F178 and F628 (shown in orange) (J, M, N). Further MBX derivatives, like MBX2319 (blue, PDB: 5ENO), MBX2931 (marine, PDB: 5ENP), and MBX3135 (slate, PDB: 5ENR), are found in an orientation highly similar to MBX3132 (K). All residues within a radius of 3.5 Å from the bound ligand are indicated in Figure 6 and assigned to their potential interaction partners in Table S1 (online only).

(residues 131–136), and the switch loop in both the AP–DBP interface as well as the short sequence between L177 and Y182, which contributes to the DBP. The flexibility provided by the loop sequences and the sum of the side chain degrees of freedom likely contribute to the enormous plasticity and multifunctionality of the internal pockets.[126]

The plasticity of the internal pockets is also reflected through the multitude of AcrB/substrate costructures. Figure 5A–G illustrates the known asymmetric structures in which substrate molecules

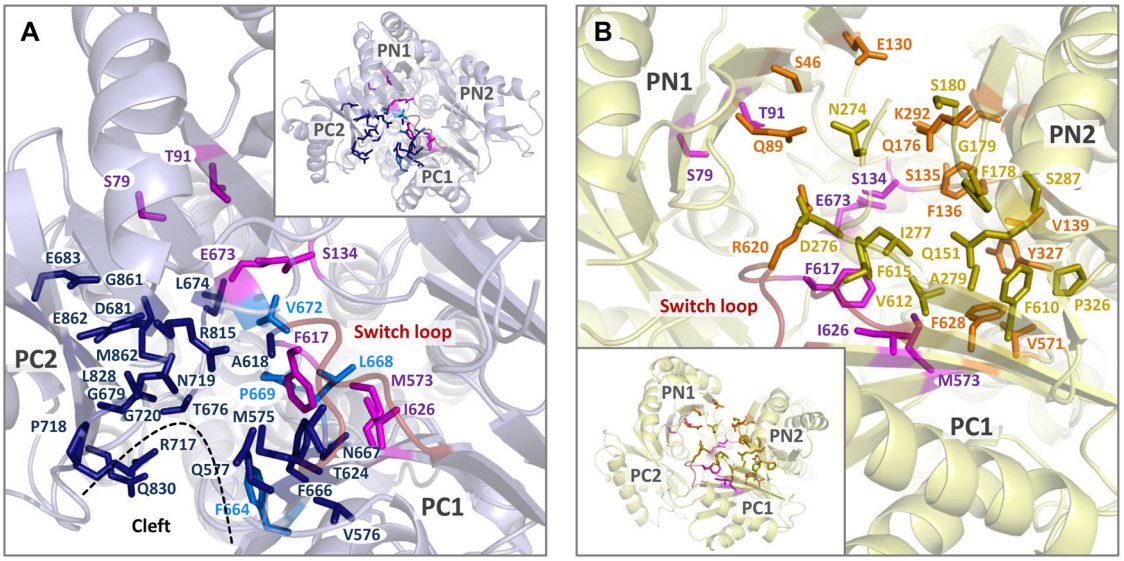

Figure 6. Residues involved in substrate binding to the AP and DBP. All residues with atoms found within a radius of 3.5 Å around one of the ligands cocrystallized with AcrB (see Fig. 5) are shown as light blue sticks for the access pocket (AP) of the L protomer (A) or as pale yellow sticks for the deep binding pocket (DBP) of the T protomer (B). Residues involved in AP substrate binding, which are part of the C-terminal porter subdomains PC1 or PC2, are shown in deep blue. Those AP residues that are exclusively found in proximity to the T bound substrate puromycin are colored marine. The residues of the AP–DBP interface located at the same height as the switch loop (indicated in red color) are highlighted in magenta (A, B). The location of some of the residues is slightly shifted as a consequence of the L–T transition. Residues that are part of the upper groove or the lower cave are shown in olive green and orange color, respectively (B). While the groove contains only residues of the N-terminal porter subdomains PN2 and PC1, the broader cave region also includes some residues of N-terminal porter subdomain PN1. Insets: Location of the PN1, PN2, PC1, and PC2 subdomains and the location of the highlighted residues with respect to the AcrB porter domain (shown in top view).

were bound in defined orientations within either the AP of the L protomer and/or the DBP in the T state. Each of the costructures can be considered as a metastable intermediate along the transport pathway of the respective substrate. These local energy minima are situated between the outer AP (DOX dimer) and the inner DBP (MIN). Higher molecular mass ligands, including RIF (PDB: 3AOB), ERY (PDB: 3AOC), and dimeric DOX (PDB: 4DX7), were bound to the L protomer, while smaller ligands, such as PUR (PDB: 5NC5), R6G (PDB: 5ENS), monomeric DOX (PDB: 4DX7), and MIN (PDB: 4DX5), were found in complex with the T state.[73,121,139,142] These local energetic minima in the AP and DBP appear to be associated with critical steps in the transport cycles of the individual substrates as suggested by competition studies with fluorescent dyes, where compounds that are likely to dwell at the same subsites interfere with each other during transport.[142,180–182] The binding of dimeric DOX to the outer AP was suggested to represent a preliminary stage to the binding of the monomeric ligand to the DBP in the sequential T conformation,[139] and might be seen as an example how the decision to finally extrude a compound is likely made in several successive steps (multistage recognition). While RIF appears to be stalled at the switch loop, ERY and PUR, which were both crystallized in a location below the switch loop (the former in the L and the latter in the T protomer), might represent states close to the conformational transition.

A closer look at the various AcrB/substrate costructures reveals how many residues are located within a radius of 3.5 Å around the individual ligands, which makes them likely to be involved in substrate binding. These residues are shown for the AP and DBP in Figure 6. A more precise subclassification of the residues into the outer and the inner AP, the AP–DBP interface at the switch loop, and the DBP groove and cave as well as an assignment of the (potentially) interacting ligands are given in

Table S1 (online only). In a direct comparison of the two internal substrate pockets, the DBP is more hydrophobic, and therefore likely has a higher affinity to the predominantly hydrophobic substrates and probably is the endpoint of their uptake.[126] However, especially for larger substrates, such as RIF, ERY, or the DOX dimer, the accessibility of the DBP within the crystallographic resolvable conformational states is limited because of constriction caused by the switch loop.[139,142] As summarized above, the stabilization of the T state is expected to be mechanistically decisive for the energization of transport.

From the comparison of the different T state costructures (Fig. 5H), the impression arises that individual substrates (MIN, DOX, R6G, and PUR) stabilize the T state by binding to different areas of the DBP. On the basis of docking[183] and MD simulations,[184] substrates are classified to preferentially bind to the upper groove, the lower cave, or both regions of the DBP (mixed binders). The groove region is formed by converging β-sheets of the PN2 and PC1 subdomains in the upper part of the DBP, while the cave (limited downward by the TMD) provides a much larger cavity. On closer examination of the computer simulations, several energetically similar binding poses were predicted. Moreover, comparison of the two X-ray AcrB/DOX costructures (PDB: 2DR6 and 4DX7) displays significantly different binding modes with approximately orthogonal ligand orientations.[136,139] Barring the possibility that the lower resolution structure prohibited the correct orientation of the bound ligand, the interaction of DOX with residues in a large pocket in several energetically *de facto* equivalent ways assumes ligands to oscillate between individual binding sites.[182] The availability of multiple binding modes would also increase the probability for a binding pocket to accommodate more than one ligand at the same time, as suggested earlier.[185]

Substrate recognition by AcrB and other proteins with multidrug binding and transport properties appears less based on a precise network of hydrogen bonds and other specific interactions than predominantly entropically driven by the hydrophobic effect (and electrostatic attraction), which is less dependent on a defined geometry.[186] However, the DBP of AcrB is not just simply hydrophobic. The ligands in the costructures mentioned above are in contact (closer than 3.5 Å) to a few very hydrophobic residues (V139, I277, and V612), but also to some charged (K292 and R620) and weakly polar residues, such as S134, Q151, Q176, and N274 (see Fig. 6). The main interaction occurs, however, by the particularly prominent aromatic residues of the phenylalanine cluster (F136, F178, F610, F615, F617, and F628) and Y327. In all, the DBP is predominantly lined by weakly hydrophobic and weakly polar residues that are predicted to create a versatile and adaptable environment with numerous so-called multifunctional sites. These dynamic local microenvironments are suggested each to provide (inducible) complementarity toward parts of the substrate structure. Accordingly, their combination is thought to result in flexible and overlapping substrate binding sites. This flexibility in interaction might also explain the high substrate promiscuity and likely facilitates efflux.[126,187]

In contrast to the binding of substrates, the potent AcrB inhibitors of the pyridopyrimidine (ABI–PP) (Fig. 5I–K) and the pyranopyridine classes (e.g., MBX3132) (Fig. 5L–N) tightly bind to the entire DBP[121,143] and were shown to significantly potentiate the activity of known antimicrobials without exhibiting membrane disruption or antibacterial activity.[188–190] Extensive interactions to both the groove and the cave region (see Table S1, online only) were suggested to prevent substrates from entering the DBP and/or conformationally arrest the protomer in the T state.[121,143] The aromatic parts of the inhibitory ligands are thereby engaged in intensive π–π stacking interactions with residues F178 and F628 (Fig. 5J–M), whereby the pyranopyridine core structures of the MBX derivatives (MBX2319, MBX2931, MBX3132, and MBX3135) show essentially similar binding properties (Fig. 5K).[121] In addition to the apparently more complex and defined binding modes of these inhibitors, including water-mediated protein–ligand interactions, computational structural analysis suggests that the binding affinities of these inhibitors significantly exceed those of AcrB substrates.[121,189] Of note, substrates also appear to bind via hydrogen bonding interaction mediated by water molecules, as is apparent for the binding of MIN, where the 1.9 Å high-resolution AcrB/MIN costructure reveals that structural water molecules support the binding of this substrate.[139]

Nevertheless, in contrast to inhibitor binding, the recognition of substrates appears to be based less

on specific interactions and more on their suitable physicochemical properties. Accordingly, for example, the residues of the phenylalanine cluster were classified as (at least partially) redundant, since individual alanine substitutions were not associated with major functional effects.[99] As an exception, the F610A substitution has been associated with more general functional impairments that, however, seem to have mechanistical causes.[129] More significant changes in substrate specificity appear to require more global changes in the properties of the binding pockets, as reflected, for example, in the comparison of the binding pockets of AcrB and AcrD.[126]

An overview of molecular determinants for substrate binding and transport

Substantial mutagenesis studies have been conducted on *acrB,* leading to amino acid residue substitutions in the AcrB protein with concomitant effects on its ability to either confer resistance to *E. coli* or its ability to transport fluorescent dyes. A dataset of 430 publications mentioning AcrB was obtained by querying the NCBI PubMed database (April 2019) for "acrb and coli" using Biopython,[191] followed by manual download of the individual papers. In the last 17 years, 50 papers have been published describing *acrB* mutagenesis or *acrB* mutants, leading to AcrB variants with wild-type-like or other than wild-type properties. Using text mining, we constructed an initial list of residues mentioned in these publications in a diverse variety of formats, such as D407 and Asp407. Manual curation of this list, combined with extraction of the observed phenotypes, resulted in a comprehensive table comprising all substitutions (from N- to C-terminus, including multiple-site exchanges) mentioned in the respective publications, and their effects on AcrB (AcrAB–TolC) activity (in percent of wild-type activity) on the tested substrates (e.g., drugs, dyes, and solvents). Activities were determined using various methods mentioned accordingly (see Table S2, online only); whenever described, the expression levels of *acrB* (or the extent of synthesis of the AcrB protein) are indicated as well. The location of the substitution is given (indication of the AcrB subdomains), as well as whether the characterized mutants were expressed from plasmid or the chromosome. Moreover, the PMID number links the substitution with the respective publication (see http://goethe.link/AcrBsubstitutions).

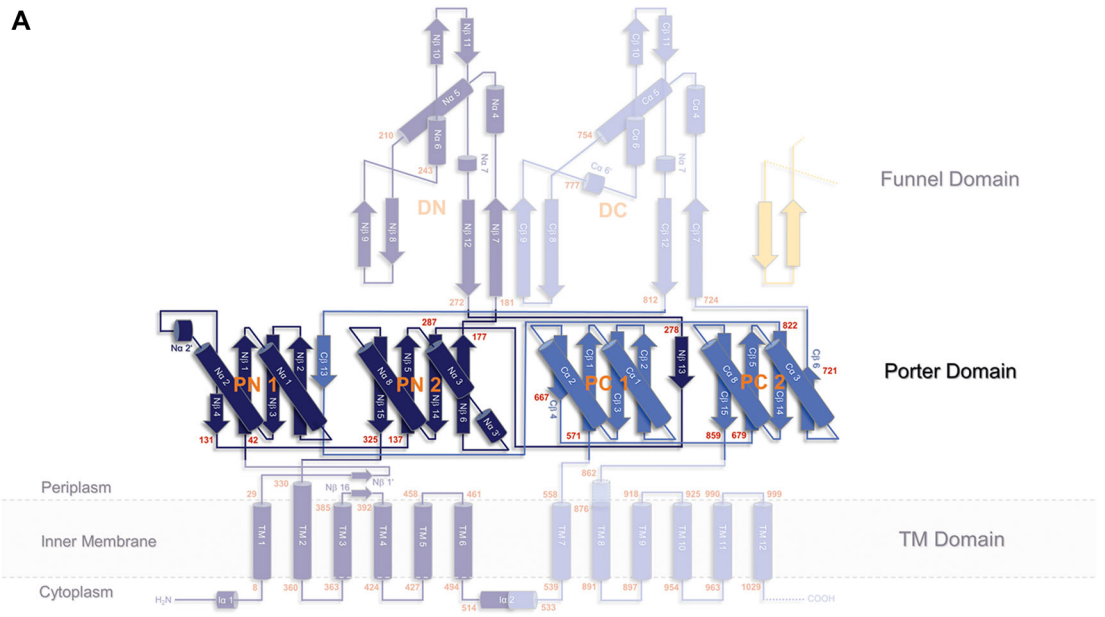

Figure 7A. **Single substitutions in the AcrB porter domain and their effects on efflux function. (A) Presents the secondary structure of an AcrB monomer with highlighted porter domain.**

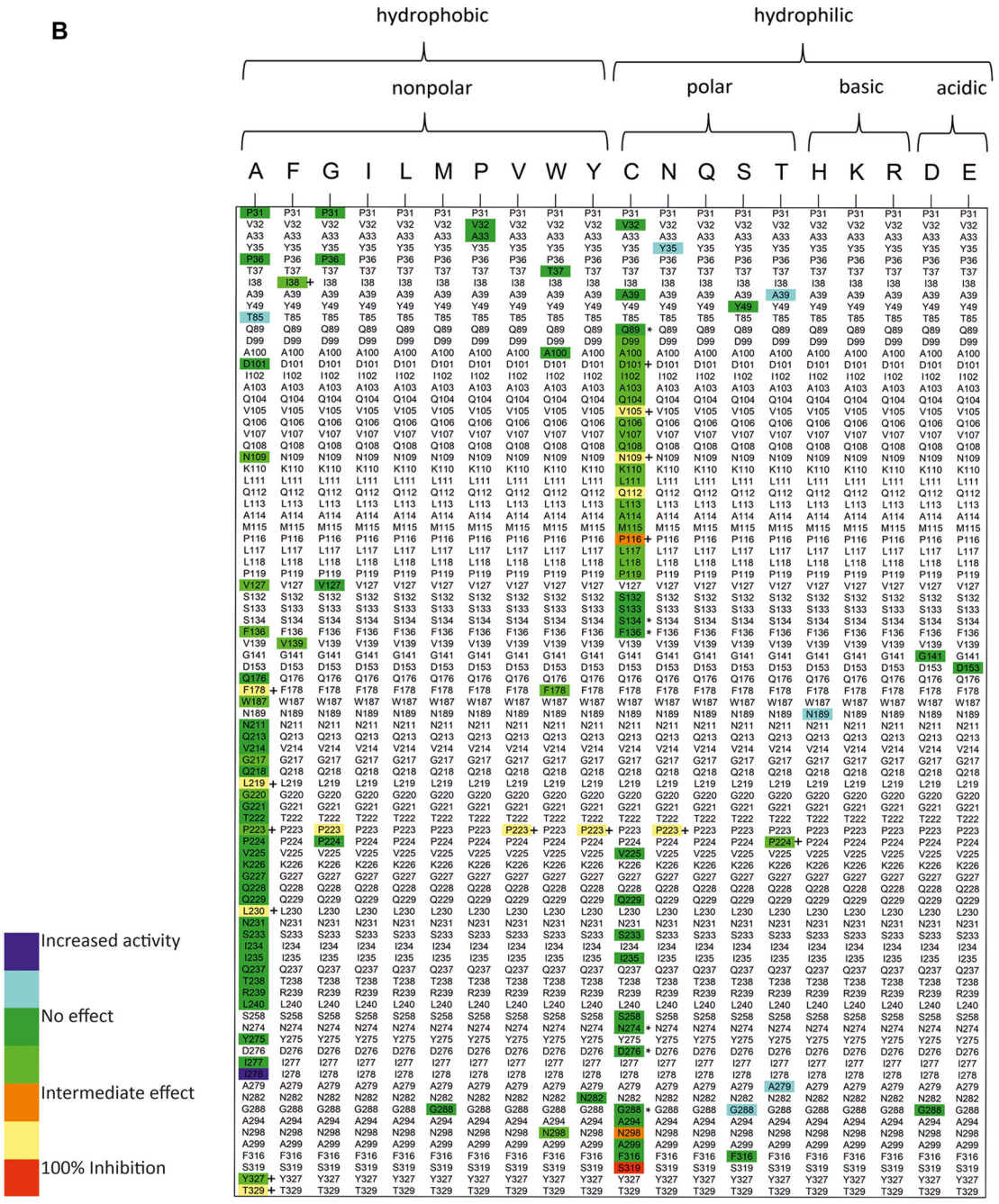

Figure 7B. (B) The heat map provides all positions (from N- to C-terminus) in the porter domain on the *Y*-axis. The substituted amino acid residues are presented on the *X*-axis, sorted by hydrophobic and hydrophilic (subdivided into polar, basic, and acidic) amino acids. Substituted positions are color coded on the basis of their activity compared with the wildtype; see legend next to the heat map. Noncolored positions were not substituted. Detailed activities, regarding the different substrates, are described in Table S2 (online only). (Positions marked with *: Cys-substitutions in wild-type AcrB background (*not* cysteine-less); positions marked with +: additional effects with regard to activities, see Table S3, online only).

We found that 235 of 1049 amino acids in AcrB were subjected to exchange, with the majority of the substitutions (65%) involving replacement for alanine and cysteine residues. Reports on deletions inside *acrB* (removal of one or more codons) have not been included in this study. To discuss the various substitutions and their effects on AcrB activity (i.e., minimal inhibitory concentration (MIC) value changes or change in dye efflux activity), we structurally divided the AcrB protein in its TMD, PD (including the AP, DBP, and switch loop), and FD (a.k.a. docking domain) (Fig. S2, online only). The effects of single-site substitutions in the TMD (Fig. S3, online only), PD (Fig. 7A), and FD (Fig. S4, online only) are displayed in color code, resulting in a heat map. AcrB is highly insensitive toward substitutions; that is, single-site exchange of amino acid residues normally does not result in a severe phenotype (compared with wild-type activity). Hence, only a few *killer mutations* (i.e., substitutions leading to an *E. coli*Δ*acrB* phenotype for all tested substrates) have been identified thus far. These substitutions are mainly located in the TMD (Table S2, online only) and include the characterized side chains involved in the binding and release of protons (transport) across the TMD (D407, D408, K940, and R971).[128,192,193] In the AcrB PD, substitutions are less detrimental, but the most prominent null phenotypes are caused by substitutions within the switch loop, which will be discussed below. One sensitive residue located in the FD, R780, was found to be important for stabilization of the AcrB protein. A suppressor mutation found by random mutagenesis within the gene encoding inactive R780A AcrB (M774K) restored the activity to almost wild-type levels.[194]

The most interesting substitutions are within the AP and DBP, as these residues are involved in the binding and/or transport of drugs (and inhibitors) (Figs. 6 and 7A). As depicted in Figure 8, we selected six residues from the AP and five residues within the DBP involved in multiple drug binding (Table S1, online only). We subsequently derived the MIC values against various antibiotics of cells harboring the indicated single-site substitution variants from Figure 7A. As shown in Figure 8, the antibiotics were sorted according to three different properties, that is, molecular weight (MW), partition coefficient (logP), and minimal projection area (MPA, the minimal rectilinear parallel projection of a surface of any shape onto a plane, see www.chemicalize.com). Two interesting observations can be made.

First, mutagenesis/substitution experiments have been made to address specific questions within the respective studies involving substitution at the indicated residues, but analysis of substrate-specific effects is lacking (or incomplete). This is emphasized in Figure 8 by the amino acid side chains of the AP colored in gray (F664C, F666C, L668C, and T676C) and the substitution effects were tested against macrolides and aminocoumarins only. Consequently, a general tendency on substrate-specific effects cannot be deduced for the AP.

Second, for the DBP, there is a tendency for larger substrates or substrates with higher MPA values to be more affected by substitutions (except macrolides). There does not appear to be a correlation between the partition coefficient (logP) of the drug and the effect of the substitution. However, to support the above claims and to identify the molecular determinants for substrate (or inhibitor) specificity, a more systematic approach is needed, including alternative descriptors of hydrophobicity. Current hypotheses on substrate selection are mostly based on assumptions and are in need of systematic and consistent experimental procedures followed by stringent analysis. Furthermore, phenotypical data obtained by characterization of AcrB variants in whole cells should be interpreted carefully for each substrate with respect to its physicochemical parameters and the outer membrane permeability.[48]

The switch loop motif separates the AP and the DBP

The 11-amino-acid–containing switch loop (residues N613–N623) is a part of the PC1 subdomain and is a drug transport modulation loop. It emerges from a β-sheet (Cβ2) with a sharp downward curvature (Fig. S5A and D, online only). According to the relative orientation, the switch loop can be structurally divided into two halves, that is, into a PC1 (N613–F617) and PN1 proximal parts (A618–N623) (Fig. S5A–C, online only).[195] The downward orientation of the PC1 proximal part of the switch loop, in the direction of the membrane plane, continues with residues G614, F615, and G616 until the peptide chain reaches F617 at the tip of the loop. From there, the loop reorients upward, including

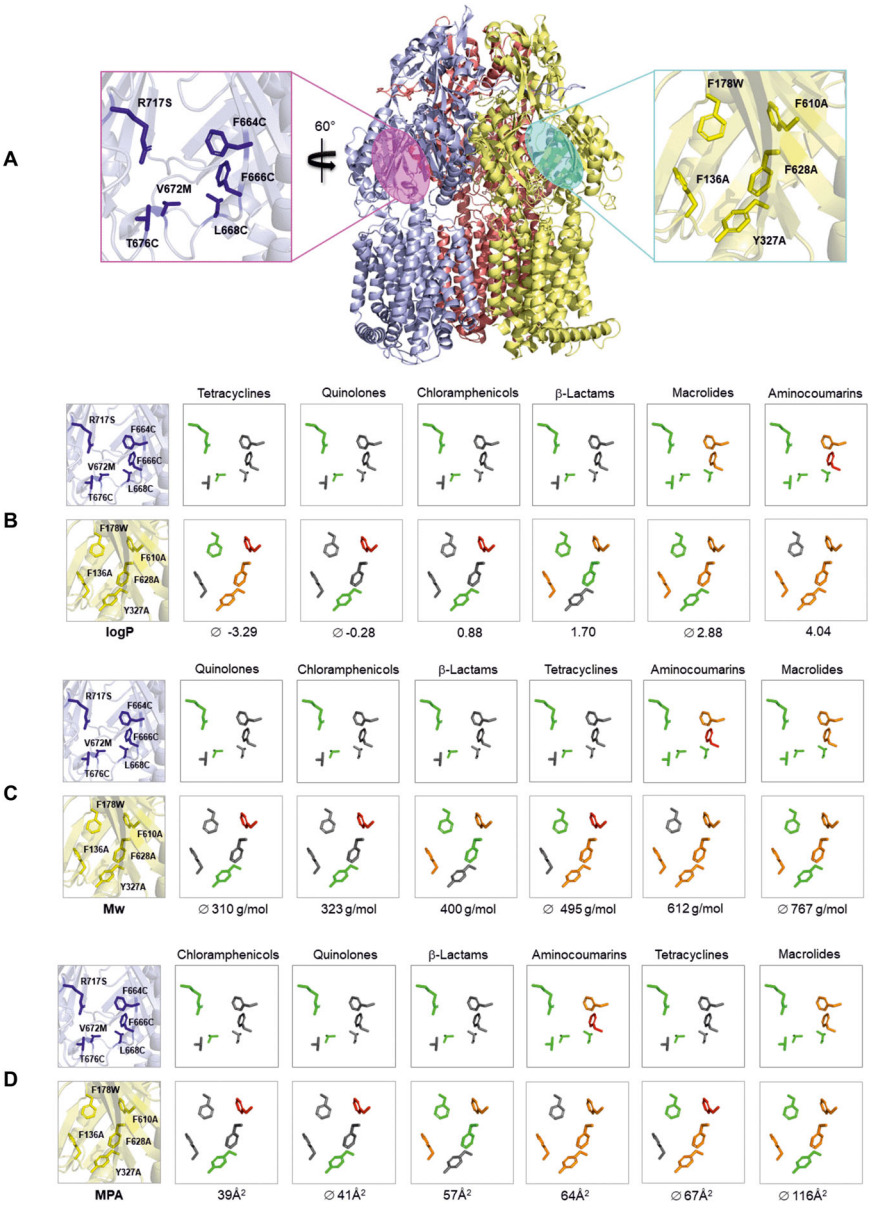

Figure 8. **Overview of substitutions in the AP and DBP of AcrB in relation to their effect on efflux function of various substrates. (A) Asymmetric AcrB (PDB: 4DX5) with the three protomers in the loose (blue), tight (yellow), and open (red) states. Enlarged views of the access pocket (AP) and the deep binding pocket (DBP) are shown to the left (AP) and right (DBP) of the trimeric AcrB structure. The AP comprises six selected residues (magenta), while the DBP comprises five selected residues (cyan). The effect on efflux of six different substrate classes, aminocoumarins (novobiocin), β-lactams (cefuroxime and oxacillin), chloramphenicols, macrolides (azithromycin, clarithromycin, and erythromycin), quinolones (levofloxacin and norfloxacin), and tetracyclines (minocycline, tetracycline, and tigecycline), are presented. The different substrate classes were sorted on the basis of the partition coefficient (logP), minimal projection area (MPA), and molecular weight (MW) (B–D). MPA, MW, and logP were averaged (Ø) for the substrate classes macrolides, quinolones, and tetracyclines, as different substrates were tested. The side chains are color coded on the basis of the effects compared with wild-type AcrB. When a substrate class was not tested, the residues are colored in gray. Green-colored side chains indicate that their substitution was without effect on activity. Orange-colored side chains showed an intermediate effect in case of substitution. This loss of activity is, in general, an effect on the minimal inhibitory concentration (MIC) by two dilution steps below the wild-type MIC, but two dilution steps above the MIC of the negative control (AcrB_D407A). Substitution of all red-colored side chains leads to the complete inhibition of AcrB.**

Ann. N.Y. Acad. Sci. 1459 (2020) 38–68 © 2019 The Authors. *Annals of the New York Academy of Sciences* published by Wiley Periodicals, Inc. on behalf of The New York Academy of Sciences.

the PN1 proximal residues A618, G619, R620, and G621. Residues Q622 and N623 form a further wider bend to connect the end of the switch loop to the antiparallel strand Cβ3. The loop motif participates in the binding of substrates to both pockets as shown by the X-ray costructures.[139,142] During the functional rotation of the individual protomers, the switch loop likewise switches between the three distinct conformational states L, T, and O. As can be seen from the comparison of the wild-type AcrB L (blue) and T (yellow) states (PDB: 4DX5), the switch loop is shifted toward the AP during the L–T transition, contributing to a larger DBP in the T state (Fig. S5D and E, online only). The comparison of different loops in the L protomer from apo, RIF, ERY, and DOX dimer (co)structures reveals a high conformational adaptability and flexibility at the tip of the loop close to F617 (Fig. S5F and G, online only). By contrast, the different T states in complex with MIN, DOX, PUR, and R6G were far more invariant when superimposed (Fig. S5H and J, online only). The switch loop contains four glycine residues, where each PC1 proximal residue (G614 and G616) faces a PN1 proximal counterpart residue (G621 and G619) in a highly symmetrical arrangement. These residues were considered of special importance for the flexibility of the loop to allow substrates to overcome the transport bottleneck between the AP and DBP.[139,142]

The observed lower inherent macrolide transport capacity of MexB[75] could be attributed to position 616 within the switch loop (Gly in AcrB, and Asn in MexB). Indeed, *E. coli* AcrB readily lost most of its macrolide transport capacity, mimicking that of MexB, by a single G616N switch loop substitution.[196] The structural characterization of this variant indicated a loop conformation in the L state that was significantly shifted toward the AP, essentially resembling the situation in the T state of the wild-type protein.[139] On the basis of the assumption that the G616N L loop (PDB: 4DX6) would collide with the DOX dimer bound to the AP of the wild-type AcrB (PDB: 4DX7), it was postulated that the G616N variant switch loop was more rigid compared with the wild-type switch loop, and that it might interfere with the uptake of larger substrates by the L protomer.[139] This finding was further corroborated, as it was shown that the G616N variant could only effectively transport substrates with a low MPA, not necessarily a property related to molecular mass (Fig. S6, online only). It supported the notion that the side chain substitution did result in a lower flexibility of the loop, rather than from involvement of the Asn side chain in preventing macrolide binding.[197]

A much stronger intervention in the loop characteristics was made when each of the two switch loop glycine residues were exchanged to proline, resulting in the symmetrical exchange variants G614P_G621P and G616P_G619P. Those variations resulted in a *de facto* inactivation of the entire efflux pump[142,195] (Fig. 7A; Figs. S5 and S7, online only). Moreover, even the G614P or G616P single-substitution variants resulted in null phenotypes (Fig. S7, online only). Surprisingly, however, substitution of the switch loop phenylalanine side chains F615 and F617 to alanine, in the Gly -> Pro background, recovered some of the activity depending on the substrate and location of the Gly -> Pro substitution. Whereas the F615A_F617A double substitution in the wild-type AcrB background only showed a major effect on sodium dodecyl sulfate (SDS) and NOV resistance (Fig. S7, online only), it rescued the G614P phenotype for ERY and TPP; for the G616P variant, however, the removal of the phenylalanine side chains (Fig. S5, online only) resulted in a rescue for almost all tested substrates (R6G, SDS, TPP, ERY, OXA, ETH, LIN, and NOV; see Fig. S7, online only). The larger rescue effect for the G616P variant might be explained by the immediate vicinity of the F615 and F617 residues flanking the proline at position 616. For the G616P_G619P double-substitution variant, the resistance phenotype was rescued as well by Ala substitutions of F615 and F617, albeit the effect (compared with the rescue phenotype of the G616P variant) was rather low (Fig. S7, online only).

Deletion of the entire switch loop also does not impair the binding of ERY, and even residual resistance activity against ERY and full activity in the presence of DOX was shown for a switch loop–less variant.[198,199] This appears somewhat in contrast compared with the nearly null-phenotype (against eight different AcrB substrates) shown for another switch loop variant,[195] but the variants are not identical and the conditions tested were different. The results shown for the switch loop thus far imply that especially its flexibility is important for optimal drug recognition and transport. Nonflexible loops

impair transport; however, this is most likely due to the obstruction of the bulky switch loop side chains (i.e., F615 and F617), as a rigidified switch loop without these bulky side chains shows the recovery of activity up to wild-type levels, depending on the tested substrate.[195]

Closing remarks

After 17 years of addressing individual questions on drug and proton recognition, we are in need of a much more systematic analysis for understanding the molecular basis of drug and proton recognition and transport. This will be, in the end, important for understanding the overall phenotype of "antibiotic resistance," where the contribution of the efflux pumps is considered not so marginal. After all, a very important basic rule applies for future directed research: understanding the fundamental principles of drug binding and transport by major efflux pumps is necessary for understanding the principles of the phenotype of multidrug resistance.

Acknowledgments

Work in the Pos lab is supported by the German Research Foundation (DFG-SFB 807, Transport and Communication across Biological Membranes and DFG-FOR2251, Adaptation and Persistence of the Emerging Pathogen *Acinetobacter baumannii*), the DFG-EXC115 (Cluster of Excellence Macromolecular Complexes at the Goethe University Frankfurt), and the Innovative Medicines Initiative Joint Undertaking Project Translocation (IMI-Translocation GA_115525). We also thank the European Union Seventh Framework Programme (FP7/2007–2013) and the European Federation of Pharmaceutical Industries and Associations (EFPIA) for in-kind contributions. M.S.K. is a recipient of a fellowship from the Friedrich-Naumann-Stiftung für die Freiheit (https://fnst.org). We also would like to thank Attilio Vargiu, Paolo Ruggerone, and Giuliano Malloci for valuable suggestions, corrections, and comments on the manuscript.

Supporting information

Additional supporting information may be found in the online version of this article.

Figure S1. Substrates of the AcrAB-TolC multidrug efflux pump.

Figure S2. Secondary structure of the AcrB monomer.

Figure S3. Single substitutions in the transmembrane (TM) Domain.

Figure S4. Single substitutions in the Funnel Domain.

Figure S5. The switch loop as a flexible structural element between AP and DBP.

Figure S6. Correlation of the substrate minimal projection area (MPA) and efflux activity of the G616N variant.

Figure S7. Switch loop subtitution causing AcrB inactivation and suppressor substitutions.

Table S1. Assignment between bound substrates and potentially interacting residues.

Table S2. http://goethe.link/AcrBsubstitutions.

Table S3. Comments on the marked positions (with a plus (+)) in the heat maps of the funnel, porter, and TM domain (Fig. 7 and Figs. S3 and S4).

Competing interests

The authors declare no competing interests.

References

1. D´Costa, V.M., C.E. King, L. Kalan, *et al*. 2011. Antibiotic resistance is ancient. *Nature* **477:** 457–461.
2. Pawlowski, A.C., W. Wang, K. Koteva, *et al*. 2016. A diverse intrinsic antibiotic resistome from a cave bacterium. *Nat. Commun.* **7:** 13803.
3. Hall, B.G. & M. Barlow. 2004. Evolution of the serine β-lactamases: past, present and future. *Drug Resist. Updat.* **7:** 111–123.
4. Grenne, T., M. Rittner, M.S. Dodd, *et al*. 2017. Evidence for early life in Earth's oldest hydrothermal vent precipitates. *Nature* **543:** 60–64.
5. Richter, D., R. Grün, R. Joannes-Boyau, *et al*. 2017. The age of the hominin fossils from Jebel Irhoud, Morocco, and the origins of the Middle Stone Age. *Nature* **546:** 293–296.
6. Perry, J., N. Waglechner & G. Wright. 2016. The prehistory of antibiotic resistance. *Cold Spring Harb. Perspect. Med.* **6:** a025197.
7. Slonczewski, J.L. & J.W. Foster. 2017. *Microbiology An Evolving Science*. W.W. Norton & Company.
8. Clardy, J., M.A. Fischbach & C.R. Currie. 2009. The natural history of antibiotics. *Curr. Biol.* **19:** R437–R441.
9. Mahajan, G.B. & L. Balachandran. 2012. Antibacterial agents from actinomycetes—a review. *Front. Biosci. (Elite Ed.)* **4:** 240–253.
10. Thaker, M.N., W. Wang, P. Spanogiannopoulos, *et al*. 2013. Identifying producers of antibacterial compounds by

screening for antibiotic resistance. *Nat. Biotechnol.* **31:** 922–927.
11. Benveniste, R. & J. Davies. 1973. Aminoglycoside antibiotic-inactivating enzymes in actinomycetes similar to those present in clinical isolates of antibiotic-resistant bacteria. *Proc. Natl. Acad. Sci. USA* **70:** 2276–2280.
12. Hopwood, D.A. 2007. How do antibiotic-producing bacteria ensure their self-resistance before antibiotic biosynthesis incapacitates them? *Mol. Microbiol.* **63:** 937–940.
13. Allen, H.K., J. Donato, H.H. Wang, *et al.* 2010. Call of the wild: antibiotic resistance genes in natural environments. *Nat. Rev. Microbiol.* **8:** 251–259.
14. Dantas, G., M.O.A. Sommer, R.D. Oluwasegun, *et al.* 2008. Bacteria subsisting on antibiotics. *Science* **320:** 100–103.
15. D'Costa, V.M., K.M. McGrann & D.W. Hughes. 2006. *et al.* Sampling the antibiotic resistome. *Science* **311:** 374–377.
16. Thomas, C.M. & K.M. Nielsen. 2005. Mechanisms of, and barriers to, horizontal gene transfer between bacteria. *Nat. Rev. Microbiol.* **3:** 711–721.
17. Forsberg, K.J., A. Reyes, B. Wang, *et al.* 2012. The shared antibiotic resistome of soil bacteria and human pathogens. *Science* **337:** 1107–1111.
18. Houndt, T. & H. Ochman. 2000. Long-term shifts in patterns of antibiotic resistance in enteric bacteria. *Appl. Environ. Microbiol.* **66:** 5406–5409.
19. Van Boeckel, T.P., C. Brower, M. Gilbert, *et al.* 2015. Global trends in antimicrobial use in food animals. *Proc. Natl. Acad. Sci. USA* **112:** 5649–5654.
20. Andersson, D.I. & D. Hughes. 2010. Antibiotic resistance and its cost: is it possible to reverse resistance? *Nat. Rev. Microbiol.* **8:** 260–271.
21. Levin, B.R., M. Lipsitch, V. Perrot, *et al.* 1997. The population genetics of antibiotic resistance. *Clin. Infect. Dis.* **24**(Suppl. 1): S9–S16.
22. Kohanski, M.A., D.J. Dwyer & J.J. Collins. 2010. How antibiotics kill bacteria: from targets to networks. *Nat. Rev. Microbiol.* **8:** 423–435.
23. Wilson, D.N. 2014. Ribosome-targeting antibiotics and mechanisms of bacterial resistance. *Nat. Rev. Microbiol.* **12:** 35–48.
24. Collin, F., S. Karkare & A. Maxwell. 2011. Exploiting bacterial DNA gyrase as a drug target: current state and perspectives. *Appl. Microbiol. Biotechnol.* **92:** 479–497.
25. Lewis, K. 2007. Persister cells, dormancy and infectious disease. *Nat. Rev. Microbiol.* **5:** 48–56.
26. Davis, B.D., L.L. Chen & P.C. Tai. 1986. Misread protein creates membrane channels: an essential step in the bactericidal action of aminoglycosides. *Proc. Natl. Acad. Sci. USA* **83:** 6164–6168.
27. Kannan, K., N. Vázquez-Laslop & A.S. Mankin. 2012. Selective protein synthesis by ribosomes with a drug-obstructed exit tunnel. *Cell* **151:** 508–520.
28. Ling, L.L., T. Schneider, A.J. Peoples, *et al.* 2015. A new antibiotic kills pathogens without detectable resistance. *Nature* **517:** 455–459.
29. Bayles, K.W. 2000. The bactericidal action of penicillin: new clues to an unsolved mystery. *Trends Microbiol.* **8:** 274–278.
30. Pohlhaus, J.R. & K.N. Kreuzer. 2005. Norfloxacin-induced DNA gyrase cleavage complexes block *Escherichia coli* replication forks, causing double-stranded breaks *in vivo*. *Mol. Microbiol.* **56:** 1416–1429.
31. Wright, G.D. 2003. Mechanisms of resistance to antibiotics. *Curr. Opin. Chem. Biol.* **7:** 563–569.
32. Blair, J.M.A., M.A. Webber, A.J. Baylay, *et al.* 2015. Molecular mechanisms of antibiotic resistance. *Nat. Rev. Microbiol.* **13:** 42–51.
33. Bush, K. 1988. Beta-lactamase inhibitors from laboratory to clinic. *Clin. Microbiol. Rev.* **1:** 109–123.
34. Waters, B. & J. Davies. 1997. Amino acid variation in the GyrA subunit of bacteria potentially associated with natural resistance to fluoroquinolone antibiotics. *Antimicrob. Agents Chemother.* **41:** 2766–2769.
35. Ruiz, J. 2003. Mechanisms of resistance to quinolones: target alterations, decreased accumulation and DNA gyrase protection. *J. Antimicrob. Chemother.* **51:** 1109–1117.
36. Jin, D.J. & C.A. Gross. 1988. Mapping and sequencing of mutations in the *Escherichia coli* rpoB gene that lead to rifampicin resistance. *J. Mol. Biol.* **202:** 45–58.
37. Hooper, D.C. & G.A. Jacoby. 2015. Mechanisms of drug resistance: quinolone resistance. *Ann. N.Y. Acad. Sci.* **1354:** 12–31.
38. Toprak, E., A. Veres, J.B. Michel, *et al.* 2012. Evolutionary paths to antibiotic resistance under dynamically sustained drug selection. *Nat. Genet.* **44:** 101–105.
39. Pu, Y., Z. Zhao, Y. Li, *et al.* 2016. Enhanced efflux activity facilitates drug tolerance in dormant bacterial cells. *Mol. Cell* **62:** 284–294.
40. Balaban, N.Q., S. Helaine, K. Lewis, *et al.* 2019. Definitions and guidelines for research on antibiotic persistence. *Nat. Rev. Microbiol.* **17:** 441–448.
41. Nolivos, S., J. Cayron, A. Dedieu, *et al.* 2019. Role of AcrAB-TolC multidrug efflux pump in drug-resistance acquisition by plasmid transfer. *Science* **364:** 778–782.
42. Fernández, L. & R.E.W. Hancock. 2012. Adaptive and mutational resistance: role of porins and efflux pumps in drug resistance. *Clin. Microbiol. Rev.* **25:** 661–681.
43. Berg, J.M., L. Stryer, J. Tymoczko, *et al.* 2019. *Biochemistry*. 9th ed. W.H. Freeman.
44. Du, D., X. Wang-Kan, A. Neuberger, *et al.* 2018. Multidrug efflux pumps: structure, function and regulation. *Nat. Rev. Microbiol.* **16:** 523–539.
45. de Cristóbal, R.E., P.A. Vincent & R.A. Salomón. 2006. Multidrug resistance pump AcrAB-TolC is required for high-level, Tet(A)-mediated tetracycline resistance in *Escherichia coli*. *J. Antimicrob. Chemother.* **58:** 31–36.
46. Tal, N. & S. Schuldiner. 2009. A coordinated network of transporters with overlapping specificities provides a robust survival strategy. *Proc. Natl. Acad. Sci. USA* **106:** 9051–9056.
47. Lee, A., W. Mao, M.S. Warren, *et al.* 2000. Interplay between efflux pumps may provide either additive or multiplicative effects on drug resistance. *J. Bacteriol.* **182:** 3142–3150.
48. Zgurskaya, H.I. & V.V. Rybenkov. 2020. Permeability barriers of Gram-negative pathogens. *Ann. N.Y. Acad. Sci.* **1459:** 5–18.
49. Nikaido, H., M. Basina, V. Nguyen, *et al.* 1998. Multidrug efflux pump AcrAB of *Salmonella typhimurium* excretes

only those β-lactam antibiotics containing lipophilic side chains. *J. Bacteriol.* **180:** 4686–4692.
50. Hassan, K.A., Q. Liu, P.J.F. Henderson & I.T. Paulsen. 2015. Homologs of the *Acinetobacter baumannii* AceI transporter represent a new family of bacterial multidrug efflux systems. *mBio* **6**. https://doi.org/10.1128/mBio.01982-14.
51. Locher, K.P. 2016. Mechanistic diversity in ATP-binding cassette (ABC) transporters. *Nat. Struct. Mol. Biol.* **23:** 487–493.
52. Nöll, A., C. Thomas, V. Herbring, *et al*. 2017. Crystal structure and mechanistic basis of a functional homolog of the antigen transporter TAP. *Proc. Natl. Acad. Sci. USA* **114:** E438–E447.
53. Zutz, A., J. Hoffmann, U.A. Hellmich, *et al*. 2011. Asymmetric ATP hydrolysis cycle of the heterodimeric multidrug ABC transport complex TmrAB from *Thermus thermophilus*. *J. Biol. Chem.* **286:** 7104–7115.
54. Fitzpatrick, A.W.P., S. Llabrés & A. Neuberger. 2017. *et al*. Structure of the MacAB–TolC ABC-type tripartite multidrug efflux pump. *Nat. Microbiol.* **2**. https://doi.org/10.1038/nmicrobiol.2017.70.
55. Schuldiner, S. 2012. Undecided membrane proteins insert in random topologies. Up, down and sideways: it does not really matter. *Trends Biochem. Sci.* **37:** 215–219.
56. Morrison, E.A., G.T. DeKoster, S. Dutta, *et al*. 2011. Antiparallel EmrE exports drugs by exchanging between asymmetric structures. *Nature* **481:** 45–50.
57. Ovchinnikov, V., T.A. Stone, C.M. Deber, *et al*. 2018. Structure of the EmrE multidrug transporter and its use for inhibitor peptide design. *Proc. Natl. Acad. Sci. USA* **115:** E7932–E7941.
58. Chen, Y.-J., O. Pornillos, S. Lieu, *et al*. 2007. X-ray structure of EmrE supports dual topology model. *Proc. Natl. Acad. Sci. USA* **104:** 18999–19004.
59. Nishino, K. & A. Yamaguchi. 2001. Analysis of a complete library of putative drug transporter genes in *Escherichia coli*. *J. Bacteriol.* **183:** 5803–5812.
60. Nasie, I., S. Steiner-Mordoch & S. Schuldiner. 2012. New substrates on the block: clinically relevant resistances for EmrE and homologues. *J. Bacteriol.* **194:** 6766–6770.
61. Dastvan, R., A.W. Fischer, S. Mishra, *et al*. 2016. Protonation-dependent conformational dynamics of the multidrug transporter EmrE. *Proc. Natl. Acad. Sci. USA* **113:** 1220–1225.
62. Zomot, E., E.H. Yardeni, A.V. Vargiu, *et al*. 2018. A new critical conformational determinant of multidrug efflux by an MFS transporter. *J. Mol. Biol.* **430:** 1368–1385.
63. Lewinson, O., J. Adler, N. Sigal, *et al*. 2006. Promiscuity in multidrug recognition and transport: the bacterial MFS Mdr transporters. *Mol. Microbiol.* **61:** 277–284.
64. Heng, J., Y. Zhao, M. Liu, *et al*. 2015. Substrate-bound structure of the *E. coli* multidrug resistance transporter MdfA. *Cell Res.* **25:** 1060–1073.
65. Miyauchi, H., S. Moriyama, T. Kusakizako, *et al*. 2017. Structural basis for xenobiotic extrusion by eukaryotic MATE transporter. *Nat. Commun.* **8:** 1633.
66. Kuroda, T. & T. Tsuchiya. 2009. Multidrug efflux transporters in the MATE family. *Biochim. Biophys. Acta* **1794:** 763–768.
67. He, X., P. Szewczyk, A. Karyakin, *et al*. 2010. Structure of a cation-bound multidrug and toxic compound extrusion transporter. *Nature* **467:** 991–994.
68. Lu, M., J. Symersky, M. Radchenko, *et al*. 2013. Structures of a Na^+-coupled, substrate-bound MATE multidrug transporter. *Proc. Natl. Acad. Sci. USA* **110:** 2099–2104.
69. Nikaido, H. 2018. RND transporters in the living world. *Res. Microbiol.* **169:** 363–371.
70. Pos, K.M. 2009. Drug transport mechanism of the AcrB efflux pump. *Biochim. Biophys. Acta* **1794:** 782–793.
71. Takatsuka, Y. & H. Nikaido. 2009. Covalently linked trimer of the AcrB multidrug efflux pump provides support for the functional rotating mechanism. *J. Bacteriol.* **191:** 1729–1737.
72. Rahman, M.M., T. Matsuo, W. Ogawa, *et al*. 2007. Molecular cloning and characterization of all RND-type efflux transporters in *Vibrio cholerae* non-O1. *Microbiol. Immunol.* **51:** 1061–1070.
73. Wang, Z., G. Fan, C.F. Hryc, *et al*. 2017. An allosteric transport mechanism for the AcrAB-TolC multidrug efflux pump. *elife* **6:** e24905.
74. Elkins, C.A. & H. Nikaido. 2002. Substrate specificity of the RND-type multidrug efflux pumps AcrB and AcrD of *Escherichia coli* is determined predominantly by the large periplasmic loops. *J. Bacteriol.* **184:** 6490–6498.
75. Tikhonova, E.B., Q. Wang & H.I. Zgurskaya. 2002. Chimeric analysis of the multicomponent multidrug efflux transporters from gram-negative bacteria. *J. Bacteriol.* **184:** 6499–6507.
76. Tseng, T.T., K.S. Gratwick, J. Kollman, *et al*. 1999. The RND permease superfamily: an ancient, ubiquitous and diverse family that includes human disease and development proteins. *J. Mol. Microbiol. Biotechnol.* **1:** 107–125.
77. Welander, P.V., R.C. Hunter, L. Zhang, *et al*. 2009. Hopanoids play a role in membrane integrity and pH homeostasis in *Rhodopseudomonas palustris* TIE-1. *J. Bacteriol.* **191:** 6145–6156.
78. Corcoran, R.B. & M.P. Scott. 2006. Oxysterols stimulate Sonic hedgehog signal transduction and proliferation of medulloblastoma cells. *Proc. Natl. Acad. Sci. USA* **103:** 8408–8413.
79. Taipale, J., M.K. Cooper, T. Maiti, *et al*. 2002. Patched acts catalytically to suppress the activity of smoothened. *Nature* **418:** 892–897.
80. Qi, X., P. Schmiege, E. Coutavas, *et al*. 2018. Two Patched molecules engage distinct sites on Hedgehog yielding a signaling-competent complex. *Science* **362:** eaas8843.
81. Qi, X., P. Schmiege, E. Coutavas, *et al*. 2018. Structures of human Patched and its complex with native palmitoylated sonic hedgehog. *Nature* **560:** 128–132.
82. Tsukazaki, T., H. Mori, Y. Echizen, *et al*. 2011. Structure and function of a membrane component SecDF that enhances protein export. *Nature* **474:** 235–238.
83. Carstea, E.D., J.A. Morris, K.G. Coleman, *et al*. 1997. Niemann–Pick C1 disease gene: homology to mediators of cholesterol homeostasis. *Science* **277:** 228–231.
84. Kumar, N., C.-C. Su, T.-H. Chou, *et al*. 2017. Crystal structures of the *Burkholderia multivorans* hopanoid transporter HpnN. *Proc. Natl. Acad. Sci. USA* **114:** 6557–6562.

85. Li, X., F. Lu, M.N. Trinh, *et al*. 2017. 3.3 Å structure of Niemann–Pick C1 protein reveals insights into the function of the C-terminal luminal domain in cholesterol transport. *Proc. Natl. Acad. Sci. USA* **114:** 9116–9121.
86. Su, C.C., P.A. Klenotic, J.R. Bolla, *et al*. 2019. MmpL3 is a lipid transporter that binds trehalose monomycolate and phosphatidylethanolamine. *Proc. Natl. Acad. Sci. USA* **116:** 11241–11246.
87. Zhang, B., J. Li, X. Yang, *et al*. 2019. Crystal structures of membrane transporter MmpL3, an anti-TB drug target. *Cell* **176:** 636–648.
88. Anes, J., M.P. McCusker, S. Fanning, *et al*. 2015. The ins and outs of RND efflux pumps in *Escherichia coli*. *Front. Microbiol.* **6:** 587.
89. Du, D., Z. Wang, N.R. James, *et al*. 2014. Structure of the AcrAB–TolC multidrug efflux pump. *Nature* **509:** 512–518.
90. Sulavik, M.C., C. Houseweart, C. Cramer, *et al*. 2001. Antibiotic susceptibility profiles of *Escherichia coli* strains lacking multidrug efflux pump genes. *Antimicrob. Agents Chemother.* **45:** 1126–1136.
91. Nichols, R.R.J., S. Sen, Y.J.Y. Choo, *et al*. 2011. Phenotypic landscape of a bacterial cell. *Cell* **144:** 143–156.
92. Baba, T., T. Ara, M. Hasegawa, *et al*. 2006. Construction of *Escherichia coli* K-12 in-frame, single-gene knockout mutants: the Keio collection. *Mol. Syst. Biol.* **2**: 2006.0008.
93. Nishino, K., T. Latifi & E.A. Groisman. 2006. Virulence and drug resistance roles of multidrug efflux systems of *Salmonella enterica* serovar Typhimurium. *Mol. Microbiol.* **59:** 126–141.
94. Lennen, R.M., M.G. Politz, M.A. Kruziki, *et al*. 2013. Identification of transport proteins involved in free fatty acid efflux in *Escherichia coli*. *J. Bacteriol.* **195:** 135–144.
95. Turlin, E., G. Heuck, M.I. Simões Brandão, *et al*. 2014. Protoporphyrin (PPIX) efflux by the MacAB-TolC pump in *Escherichia coli*. *Microbiologyopen* **3:** 849–859.
96. Yamanaka, H., H. Kobayashi, E. Takahashi, *et al*. 2008. MacAB is involved in the secretion of *Escherichia coli* heat-stable enterotoxin II. *J. Bacteriol.* **190:** 7693–7698.
97. Lu, S. & H.I. Zgurskaya. 2013. MacA, a periplasmic membrane fusion protein of the macrolide transporter MacAB-TolC, binds lipopolysaccharide core specifically and with high affinity. *J. Bacteriol.* **195:** 4865–4872.
98. Tsukagoshi, N. & R. Aono. 2000. Entry into and release of solvents by *Escherichia coli* in an organic-aqueous two-liquid-phase system and substrate specificity of the AcrAB-TolC solvent-extruding pump. *J. Bacteriol.* **182:** 4803–4810.
99. Bohnert, J.A., S. Schuster, M.A. Seeger, *et al*. 2008. Site-directed mutagenesis reveals putative substrate binding residues in the *Escherichia coli* RND efflux pump AcrB. *J. Bacteriol.* **190:** 8225–8229.
100. Kobayashi, N., N. Tamura, H.W. Van Veen, *et al*. 2014. β-Lactam selectivity of multidrug transporters AcrB and AcrD resides in the proximal binding pocket. *J. Biol. Chem.* **289:** 10680–10690.
101. Nishino, K., J. Yamada, H. Hirakawa, *et al*. 2003. Roles of TolC-dependent multidrug transporters of *Escherichia coli* in resistance to β-lactams. *Antimicrob. Agents Chemother.* **47:** 3030–3033.
102. Rosenberg, E.Y., D. Ma & H. Nikaido. 2000. AcrD of *Escherichia coli* is an aminoglycoside efflux pump. *J. Bacteriol.* **182:** 1754–1756.
103. Ruggerone, P., A.V. Vargiu, F. Collu, *et al*. 2013. Molecular dynamics computer simulations of multidrug RND efflux pumps. *Comput. Struct. Biotechnol. J.* **5:** e201302008.
104. Ramaswamy, V.K., A.V. Vargiu, G. Malloci, *et al*. 2018. Molecular determinants of the promiscuity of MexB and MexY multidrug transporters of *Pseudomonas aeruginosa*. *Front. Microbiol.* **9:** 1144.
105. Hirakawa, H., Y. Inazumi, T. Masaki, *et al*. 2005. Indole induces the expression of multidrug exporter genes in *Escherichia coli*. *Mol. Microbiol.* **55:** 1113–1126.
106. Nagano, K. & H. Nikaido. 2009. Kinetic behavior of the major multidrug efflux pump AcrB of *Escherichia coli*. *Proc. Natl. Acad. Sci. USA* **106:** 5854–5858.
107. Verchère, A., M. Dezi, V. Adrien, *et al*. 2015. *In vitro* transport activity of the fully assembled MexAB-OprM efflux pump from *Pseudomonas aeruginosa*. *Nat. Commun.* **6:** https://doi.org/10.1038/ncomms7890.
108. Li, X.Z., P. Plésiat & H. Nikaido. 2015. The challenge of efflux-mediated antibiotic resistance in Gram-negative bacteria. *Clin. Microbiol. Rev.* **28:** 337–418.
109. Blair, J.M.A., H.E. Smith, V. Ricci, *et al*. 2015. Expression of homologous RND efflux pump genes is dependent upon AcrB expression: implications for efflux and virulence inhibitor design. *J. Antimicrob. Chemother.* **70:** 424–431.
110. Piddock, L.J. 2006. Clinically relevant chromosomally encoded multidrug resistance efflux pumps in bacteria. *Clin. Microbiol. Rev.* **19:** 382–402.
111. Hong, B.K., M. Wang, H.P. Chi, *et al*. 2009. oqxAB encoding a multidrug efflux pump in human clinical isolates of Enterobacteriaceae. *Antimicrob. Agents Chemother.* **53:** 3582–3584.
112. Ho, P.L., K. Ng, W. Lo, *et al*. 2016. Plasmid-mediated OqxAB is an important mechanism for nitrofurantoin resistance in *Escherichia coli*. *Antimicrob. Agents Chemother.* **60:** 537–543.
113. Ricci, V., P. Tzakas, A. Buckley, *et al*. 2006. Ciprofloxacin-resistant *Salmonella enterica* serovar Typhimurium strains are difficult to select in the absence of AcrB and TolC. *Antimicrob. Agents Chemother.* **50:** 38–42.
114. Vargiu, A.V., K.M. Pos, K. Poole, *et al*. 2016. Editorial: Bad bugs in the XXIst century: resistance mediated by multidrug efflux pumps in gram-negative bacteria. *Front. Microbiol.* **7:** 833.
115. Long, H., S.F. Miller, C. Strauss, *et al*. 2016. Antibiotic treatment enhances the genome-wide mutation rate of target cells. *Proc. Natl. Acad. Sci. USA* **113:** E2498–E2505.
116. Hancock, R.E.W. & D.S. Chapple. 1999. Peptide antibiotics. *Antimicrob. Agents Chemother.* **43:** 1317–1323.
117. Tacconelli, E., E. Carrara, A. Savoldi, *et al*. 2018. Discovery, research, and development of new antibiotics: the WHO priority list of antibiotic-resistant bacteria and tuberculosis. *Lancet Infect. Dis.* **18:** 318–327.
118. Nang, S.C., J. Li & T. Velkov. 2019. The rise and spread of *mcr* plasmid-mediated polymyxin resistance. *Crit. Rev. Microbiol.* **45:** 131–161.

119. Renau, T.E., R. Léger, E.M. Flamme, *et al*. 1999. Inhibitors of efflux pumps in *Pseudomonas aeruginosa* potentiate the activity of the fluoroquinolone antibacterial levofloxacin. *J. Med. Chem.* **42:** 4928–4931.
120. Venter, H., R. Mowla, T. Ohene-Agyei, *et al*. 2015. RND-type drug efflux pumps from Gram-negative bacteria: molecular mechanism and inhibition. *Front. Microbiol.* **6:** 377.
121. Sjuts, H., A.V. Vargiu, S.M. Kwasny, *et al*. 2016. Molecular basis for inhibition of AcrB multidrug efflux pump by novel and powerful pyranopyridine derivatives. *Proc. Natl. Acad. Sci. USA* **113:** 3509–3514.
122. Daury, L., F. Orange, J.-C. Taveau, *et al*. 2016. Tripartite assembly of RND multidrug efflux pumps. *Nat. Commun.* **7:** 10731.
123. Tsutsumi, K., R. Yonehara, E. Ishizaka-Ikeda, *et al*. 2019. Structures of the wild-type MexAB–OprM tripartite pump reveal its complex formation and drug efflux mechanism. *Nat. Commun.* **10:** 1520.
124. López, C.A., T. Travers, K.M. Pos, *et al*. 2017. Dynamics of intact MexAB-OprM efflux pump: focusing on the MexA–OprM interface. *Sci. Rep.* **7:** 16521.
125. Fischer, N. & C. Kandt. 2013. Porter domain opening and closing motions in the multi-drug efflux transporter AcrB. *Biochim. Biophys. Acta* **1828:** 632–641.
126. Ramaswamy, V.K., A.V. Vargiu, G. Malloci, *et al*. 2017. Molecular rationale behind the differential substrate specificity of bacterial RND multi-drug transporters. *Sci. Rep.* **7:** 8075.
127. Vargiu, A.V. & H. Nikaido. 2012. Multidrug binding properties of the AcrB efflux pump characterized by molecular dynamics simulations. *Proc. Natl. Acad. Sci. USA* **109:** 20637–20642.
128. Eicher, T., M.A. Seeger, C. Anselmi, *et al*. 2014. Coupling of remote alternating-access transport mechanisms for protons and substrates in the multidrug efflux pump AcrB. *elife* **3:** e03145.
129. Vargiu, A.V., F. Collu, R. Schulz, *et al*. 2011. Effect of the F610A mutation on substrate extrusion in the AcrB transporter: explanation and rationale by molecular dynamics simulations. *J. Am. Chem. Soc.* **133:** 10704–10707.
130. Yue, Z., W. Chen, H.I. Zgurskaya, *et al*. 2017. Constant pH molecular dynamics reveals how proton release drives the conformational transition of a transmembrane efflux pump. *J. Chem. Theory Comput.* **13:** 6405–6414.
131. Zuo, Z., J. Weng & W. Wang. 2016. Insights into the inhibitory mechanism of D13-9001 to the multidrug transporter AcrB through molecular dynamics simulations. *J. Phys. Chem. B* **120:** 2145–2154.
132. Atzori, A., V.N. Malviya, G. Malloci, *et al*. 2019. Identification and characterization of carbapenem binding sites within the RND-transporter AcrB. *Biochim. Biophys. Acta Biomembr.* **1861:** 62–74.
133. Vargiu, A.V., V.K. Ramaswamy, I. Malvacio, *et al*. 2018. Water-mediated interactions enable smooth substrate transport in a bacterial efflux pump. *Biochim. Biophys. Acta Gen. Subj.* **1862:** 836–845.
134. Murakami, S., R. Nakashima, E. Yamashita, *et al*. 2002. Crystal structure of bacterial multidrug efflux transporter AcrB. *Nature* **419:** 587–593.
135. Su, C.C., M. Li, R. Gu, *et al*. 2006. Conformation of the AcrB multidrug efflux pump in mutants of the putative proton relay pathway. *J. Bacteriol.* **188:** 7290–7296.
136. Murakami, S., R. Nakashima, E. Yamashita, *et al*. 2006. Crystal structures of a multidrug transporter reveal a functionally rotating mechanism. *Nature* **443:** 173–179.
137. Seeger, M.A., A. Schiefner, T. Eicher, *et al*. 2006. Structural asymmetry of AcrB trimer suggests a peristaltic pump mechanism. *Science* **313:** 1295–1298.
138. Sennhauser, G., P. Amstutz, C. Briand, *et al*. 2007. Drug export pathway of multidrug exporter AcrB revealed by DARPin inhibitors. *PLoS Biol.* **5:** 0106–0113.
139. Eicher, T., H.-J. Cha, M.A. Seeger, *et al*. 2012. Transport of drugs by the multidrug transporter AcrB involves an access and a deep binding pocket that are separated by a switch-loop. *Proc. Natl. Acad. Sci. USA* **109:** 5687–5692.
140. Boyer, P.D. 1997. The ATP synthase—a splendid molecular machine. *Annu. Rev. Biochem.* **66:** 717–749.
141. Seeger, M.A., K. Diederichs, T. EIcher, *et al*. 2008. The AcrB efflux pump: conformational cycling and persistalsis lead to multidrug resistance. *Curr. Drug Targets* **9:** 729–749.
142. Nakashima, R., K. Sakurai, S. Yamasaki, *et al*. 2011. Structures of the multidrug exporter AcrB reveal a proximal multisite drug-binding pocket. *Nature* **480:** 566–569.
143. Nakashima, R., K. Sakurai, S. Yamasaki, *et al*. 2013. Structural basis for the inhibition of bacterial multidrug exporters. *Nature* **500:** 102–106.
144. Brandstätter, L., L. Sokolova, T. Eicher, *et al*. 2011. Analysis of AcrB and AcrB/DARPin ligand complexes by LILBID MS. *Biochim. Biophys. Acta* **1808:** 2189–2196.
145. Yu, L., W. Lu & Y. Wei. 2011. AcrB trimer stability and efflux activity, insight from mutagenesis studies. *PLoS One* **6:** e28390.
146. Hobbs, E.C., X. Yin, B.J. Paul, *et al*. 2012. Conserved small protein associates with the multidrug efflux pump AcrB and differentially affects antibiotic resistance. *Proc. Natl. Acad. Sci. USA* **109:** 16696–16701.
147. Törnroth-Horsefield, S., P. Gourdon, R. Horsefield, *et al*. 2007. Crystal structure of AcrB in complex with a single transmembrane subunit reveals another twist. *Structure* **15:** 1663–1673.
148. Zgurskaya, H.I. & H. Nikaido. 1999. AcrA is a highly asymmetric protein capable of spanning the periplasm. *J. Mol. Biol.* **285:** 409–420.
149. Yoneyama, H., H. Maseda, H. Kamiguchi, *et al*. 2000. Function of the membrane fusion protein, MexA, of the MexA, B-OprM efflux pump in *Pseudomonas aeruginosa* without an anchoring membrane. *J. Biol. Chem.* **275:** 4628–4634.
150. Higgins, M.K., E. Bokma, E. Koronakis, *et al*. 2004. Structure of the periplasmic component of a bacterial drug efflux pump. *Proc. Natl. Acad. Sci. USA* **101:** 9994–9999.
151. Akama, H., T. Matsuura, S. Kashiwagi, *et al*. 2004. Crystal structure of the membrane fusion protein, MexA, of the multidrug transporter in *Pseudomonas aeruginosa*. *J. Biol. Chem.* **279:** 25939–25942.
152. Mikolosko, J., K. Bobyk, H.I. Zgurskaya, *et al*. 2006. Conformational flexibility in the multidrug efflux system protein AcrA. *Structure* **14:** 577–587.
153. Symmons, M.F., E. Bokma, E. Koronakis, *et al*. 2009. The assembled structure of a complete tripartite bacterial

multidrug efflux pump. *Proc. Natl. Acad. Sci. USA* **106:** 7173–7178.
154. Xu, Y., A. Moeller, S.Y. Jun, *et al*. 2012. Assembly and channel opening of outer membrane protein in tripartite drug efflux pumps of gram-negative bacteria. *J. Biol. Chem.* **287:** 11740–11750.
155. Su, C.C., F. Long, M.T. Zimmermann, *et al*. 2011. Crystal structure of the CusBA heavy-metal efflux complex of *Escherichia coli*. *Nature* **470:** 558–562.
156. Jeong, H., J.S. Kim, S. Song, *et al.* 2016. Pseudoatomic structure of the tripartite multidrug efflux pump AcrAB-TolC reveals the intermeshing cogwheel-like interaction BETWEEN AcrA and TolC. *Structure* **24:** 272–276.
157. Zgurskaya, H.I., G. Krishnamoorthy, A. Ntreh, *et al*. 2011. Mechanism and function of the outer membrane channel TolC in multidrug resistance and physiology of Enterobacteria. *Front. Microbiol.* **2:** 189.
158. Bennion, D., E.S. Charlson, E. Coon, *et al*. 2010. Dissection of β-barrel outer membrane protein assembly pathways through characterizing BamA POTRA 1 mutants of *Escherichia coli*. *Mol. Microbiol.* **77:** 1153–1171.
159. Koronakis, V., A. Sharff, E. Koronakis, *et al*. 2000. Crystal structure of the bacterial membrane protein TolC central to multidrug efflux and protein export. *Nature* **405:** 914–919.
160. Andersen, C., E. Koronakis, E. Bokma, *et al.* 2002. Transition to the open state of the TolC periplasmic tunnel entrance. *Proc. Natl. Acad. Sci. USA* **99:** 11103–11108.
161. Bavro, V.N., Z. Pietras, N. Furnham, *et al*. 2008. Assembly and channel opening in a bacterial drug efflux machine. *Mol. Cell* **30:** 114–121.
162. Pei, X.-Y., P. Hinchliffe, M.F. Symmons, *et al*. 2011. Structures of sequential open states in a symmetrical opening transition of the TolC exit duct. *Proc. Natl. Acad. Sci. USA* **108:** 2112–2117.
163. Kim, J.-S., H. Jeong, S. Song, *et al.* 2015. Structure of the tripartite multidrug efflux pump AcrAB-TolC suggests an alternative assembly mode. *Mol. Cells* **38:** 180–186.
164. Neuberger, A., D. Du & B.F. Luisi. 2018. Structure and mechanism of bacterial tripartite efflux pumps. *Res. Microbiol.* **169:** 401–413.
165. Ntsogo Enguéné, V.Y., A. Verchère, G. Phan, *et al*. 2015. Catch me if you can: a biotinylated proteoliposome affinity assay for the investigation of assembly of the MexA-MexB-OprM efflux pump from *Pseudomonas aeruginosa*. *Front. Microbiol.* **6:** 541.
166. Kralj, J.M., D.R. Hochbaum, A.D. Douglass, *et al*. 2011. Electrical spiking in *Escherichia coli* probed with a fluorescent voltage-indicating protein. *Science* **333:** 345–348.
167. Müller, R.T. & K.M. Pos. 2015. The assembly and disassembly of the AcrAB-TolC three-component multidrug efflux pump. *Biol. Chem.* **396:** 1083–1089.
168. Tamura, N., S. Murakami, Y. Oyama, *et al.* 2005. Direct interaction of multidrug efflux transporter AcrB and outer membrane channel TolC detected via site-directed disulfide cross-linking. *Biochemistry* **44:** 11115–11121.
169. Lu, W., M. Zhong & Y. Wei. 2011. Folding of AcrB subunit precedes trimerization. *J. Mol. Biol.* **411:** 264–274.
170. Qiu, W., Z. Fu, G.G. Xu, *et al*. 2018. Structure and activity of lipid bilayer within a membrane-protein transporter. *Proc. Natl. Acad. Sci. USA* **115:** 12985–12990.
171. Yu, E.W., J.R.J.R. Aires & H. Nikaido. 2003. AcrB multidrug efflux pump of *Escherichia coli*: composite substrate-binding cavity of exceptional flexibility generates its extremely wide substrate specificity. *J. Bacteriol.* **185:** 5657–5664.
172. Hung, L.W., H.B. Kim, S. Murakami, *et al*. 2013. Crystal structure of AcrB complexed with linezolid at 3.5 Å resolution. *J. Struct. Funct. Genomics* **14:** 71–75.
173. Zwama, M., S. Yamasaki, R. Nakashima, *et al.* 2018. Multiple entry pathways within the efflux transporter AcrB contribute to multidrug recognition. *Nat. Commun.* **9:** 124.
174. Seeger, M.A., C. von Ballmoos, T. Eicher, *et al*. 2008. Engineered disulfide bonds support the functional rotation mechanism of multidrug efflux pump AcrB. *Nat. Struct. Mol. Biol.* **15:** 199–205.
175. Lim, S.P. & H. Nikaido. 2010. Kinetic parameters of efflux of penicillins by the multidrug efflux transporter AcrAB-TolC of *Escherichia coli*. *Antimicrob. Agents Chemother.* **54:** 1800–1806.
176. Oswald, C., H.-K. Tam & K.M. Pos. 2016. Transport of lipophilic carboxylates is mediated by transmembrane helix 2 in multidrug transporter AcrB. *Nat. Commun.* **7:** 13819.
177. Kim, H.S., D. Nagore & H. Nikaido. 2010. Multidrug efflux pump MdtBC of *Escherichia coli* is active only as a B_2C heterotrimer. *J. Bacteriol.* **192:** 1377–1386.
178. Kim, H.S. & H. Nikaido. 2012. Different functions of MdtB and MdtC subunits in the heterotrimeric efflux transporter MdtB2C complex of *Escherichia coli*. *Biochemistry* **51:** 4188–4197.
179. Su, C.-C., L. Yin, N. Kumar, *et al*. 2017. Structures and transport dynamics of a *Campylobacter jejuni* multidrug efflux pump. *Nat. Commun.* **8:** 171.
180. Bohnert, J.A., B. Karamian & H. Nikaido. 2010. Optimized Nile Red efflux assay of AcrAB-TolC multidrug efflux system shows competition between substrates. *Antimicrob. Agents Chemother.* **54:** 3770–3775.
181. Iyer, R., A. Ferrari, R. Rijnbrand, *et al*. 2015. A fluorescent microplate assay quantifies bacterial efflux and demonstrates two distinct compound binding sites in AcrB. *Antimicrob. Agents Chemother.* **59:** 2388–2397.
182. Yamaguchi, A., R. Nakashima & K. Sakurai. 2015. Structural basis of RND-type multidrug exporters. *Front. Microbiol.* **6:** 327.
183. Takatsuka, Y., C. Chen & H. Nikaido. 2010. Mechanism of recognition of compounds of diverse structures by the multidrug efflux pump AcrB of *Escherichia coli*. *Proc. Natl. Acad. Sci. USA* **107:** 6559–6565.
184. Vargiu, A.V. & H. Nikaido. 2012. Multidrug binding properties of the AcrB efflux pump characterized by molecular dynamics simulations. *Proc. Natl. Acad. Sci. USA* **109:** 20637–20642.
185. Kinana, A.D., A.V. Vargiu & H. Nikaido. 2013. Some ligands enhance the efflux of other ligands by the *Escherichia coli* multidrug pump AcrB. *Biochemistry* **52:** 8342–8351.

186. Neyfakh, A.A. 2002. Mystery of multidrug transporters: the answer can be simple. *Mol. Microbiol.* **44:** 1123–1130.
187. Imai, T., N. Miyashita, Y. Sugita, *et al*. 2011. Functionality mapping on internal surfaces of multidrug transporter AcrB based on molecular theory of solvation: implications for drug efflux pathway. *J. Phys. Chem. B* **115:** 8288–8295.
188. Yoshida, K., K. Nakayama, M. Ohtsuka, *et al*. 2007. MexAB-OprM specific efflux pump inhibitors in *Pseudomonas aeruginosa*. Part 7: highly soluble and *in vivo* active quaternary ammonium analogue D13-9001, a potential preclinical candidate. *Bioorg. Med. Chem*. **15:** 7087–7097.
189. Vargiu, A.V., P. Ruggerone, T.J. Opperman, *et al*. 2014. Molecular mechanism of MBX2319 inhibition of *Escherichia coli* AcrB multidrug efflux pump and comparison with other inhibitors. *Antimicrob. Agents Chemother.* **58:** 6224–6234.
190. Opperman, T.J., S.M. Kwasny, H.-S. Kim, *et al*. 2014. Characterization of a novel pyranopyridine inhibitor of the AcrAB efflux pump of *Escherichia coli*. *Antimicrob. Agents Chemother.* **58:** 722–733.
191. Cock, P.J.A., T. Antao, J.T. Chang, *et al*. 2009. Biopython: freely available Python tools for computational molecular biology and bioinformatics. *Bioinformatics* **25:** 1422–1423.
192. Takatsuka, Y. & H. Nikaido. 2006. Threonine-978 in the transmembrane segment of the multidrug efflux pump AcrB of *Escherichia coli* is crucial for drug transport as a probable component of the proton relay network. *J. Bacteriol.* **188:** 7284–7289.
193. Seeger, M.A., C. von Ballmoos, F. Verrey, *et al*. 2009. Crucial role of Asp408 in the proton translocation pathway of multidrug transporter AcrB: evidence from site-directed mutagenesis and carbodiimide labeling. *Biochemistry* **48:** 5801–5812.
194. Yu, L., W. Lu, C. Ye, *et al*. 2013. Role of a conserved residue R780 in *Escherichia coli* multidrug transporter AcrB. *Biochemistry* **52:** 6790–6796.
195. Müller, R.T., T. Travers, H.J. Cha, *et al*. 2017. Switch loop flexibility affects substrate transport of the AcrB efflux pump. *J. Mol. Biol.* **429:** 3863–3874.
196. Wehmeier, C., S. Schuster, E. Fähnrich, *et al*. 2009. Site-directed mutagenesis reveals amino acid residues in the *Escherichia coli* RND efflux pump AcrB that confer macrolide resistance. *Antimicrob. Agents Chemother.* **53:** 329–330.
197. Cha, H.J., R.T. Müller & K.M. Pos. 2014. Switch-loop flexibility affects transport of large drugs by the promiscuous AcrB multidrug efflux transporter. *Antimicrob. Agents Chemother.* **58:** 4767–4772.
198. Ababou, A. & V. Koronakis. 2016. Structures of gate loop variants of the AcrB drug efflux pump bound by erythromycin substrate. *PLoS One* **11:** e0159154.
199. Ababou, A. 2018. New insights into the structural and functional involvement of the gate loop in AcrB export activity. *Biochim. Biophys. Acta Proteins Proteom.* **1866:** 242–253.
200. Hayashi K., R. Nakashima, K. Sakurai, et al. 2015. AcrB–AcrA fusion proteins that act as multidrug efflux transporters. *J. Bacteriol*. **198:** 332–342.